Preface

This volume is a collection of reports from the 16th TRACE conference “Tree Rings in Archaeology, Climatology and Ecology” organized by the Siberian Federal University, Baltic Federal University, Russian Scientific Foundation and by the initiative of the ‘Association for Tree-Ring Research’ (ATR).

Scientists from 16 countries (Spain, Germany, Italy, Switzerland, Netherland, Estonia, Belarus, Belgium, Slovenia, Czech Republic, Poland, Romania, Denmark, Kyrgyz Republic, Serbia and Russia) came to the most western part of Russia, Kaliningrad region in May 16th – 21th, 2017. The participants presented 39 talks and 42 posters at six thematic sections: “Forests and climate change”, “Tree-line change”, “Studies on Climate-Growth Relationships”, “Methodological Issues on Climate-Growth Relationships and Long-Term Reconstructions”, “High-Resolution Information on Climate-Growth Relationships”, “Hydrology Related to Anatomical Structure and Mortality”.

Many of the participants also participated in four workshops: “R Fundamentals in Dendrochronology” by E. van der Maaten, “Methods of Quantitative and Functional Wood Anatomy” by G. von Arx and P. Fonti, “Process Modeling” by V. Shishov, “Detecting Climate-Growth Relationships by use of the Statistical Analysis Tool CLIMTREG” by W. Beck. In the midst of the conference, the participants enjoyed the outdoor conference session at the Curonian Spit National Park that is a UNESCO World Heritage Site.

TRACE 2017 was the first TRACE conference held in Russia. We enjoyed very much gathering so many early career and experienced researchers and helping to communicate and share skills, ideas and high spirit of science. The conference has provided a unique possibility for Russian early career researchers to meet new colleagues and establish promising professional connections. We are very thankful to all the participants for creating such atmosphere at TRACE2017.

This TRACE 2017 volume no.16 is the last volume printed as “independent” proceedings volume. This series now ends. This is not the end of the TRACE-tradition, but the start of a new series of special issues “TRACE 20XX” in “Dendrochronologia”.

This 16th and last proceedings volume comprises 6 short papers. These papers are giving a very brief but valuable representation of the conference scientific content and we would like to express our gratitude to the authors for contributing to the TRACE2017 volume, and the reviewers for their very important efforts in making the manuscripts better.

Irina Sviderskaya
Gerd Helle
Holger Gärtner

CONTENTS

SECTION Ω

SECTION Ω

Types of ecological tree-lines on the Dalniy Taganay Mountain in the Southern Urals

M.A. Gurskaya, V.V. Kukarskyh, A.A. Grigoriev & M.O. Bubnov

Institute of Plant and Animal Ecology, UB Russian Academy of sciences, Ekaterinburg
E-mail: mgurskaya@yandex.ru

Introduction

The upper tree-line is the most important biogeographical boundary of tree distribution in mountainous environments. The upper tree-line can be differentiated in three ways. First, 'species tree-lines' are characterized by different tree species composition, for example, there exist birch, larch, or spruce tree-lines, which vary with mesoclimatic growth conditions. Second, 'ecological tree-lines' are based on environmental factors and topographic complexity, and are characterised by uniform species composition but located at different elevations and on slopes of different expose within a ridge. Third, 'anthropogenic tree-lines' form in response to a variety of human activities and are located below the natural upper tree-line distribution (Gorchakovsky & Shiyatov 1985).
In recent years, researchers have focused on the study of spatiotemporal dynamics of forest stands under temperature-limiting conditions (Mazepa 2005, Danby & Hik 2007, Kullman & Öberg 2009, Moiseev et al. 2010). However, temperature is not the only driver of upper tree-line dynamics in mountain settings. Environmental drivers controlling upper tree-line variability are numerous including topographic complexity such as slope exposure, steepness, direction of prevalent winds, snow accumulation, snow pack depth and soil conditions. Therefore, inter-and intraspecies spatiotemporal dynamics of tree-line species can vary on a single mountain top. The purpose of this work is to identify the main ecological types of the upper tree-lines at the Dalniy Taganay Mountain in the Southern Urals.

Methods

Study area

The Taganay Ridge is 52 km long and is located in the northern part of the Southern Ural Mountains. Tectonically the ridge lies within the Ural-Tau, the Central Ural rise of the Taganay-Ufaley anticlinorium, where the Taganay suite of geological deposits of the Upper Proterozoic is separated with outcrops of intrusive rocks. We chose the Dalniy Taganay Mountain (DTM) at theTaganay ridge as the site is the most remoted from anthropogenic activity (Fig.1). The DTM has steep slopes and consists of three ridges. The western summit is composed of crystalline mica shale rocks and has an elevation of 1146 m above sea level (a.s.l.). The central top consists entirely of quartzite (taganait) and forms a large plateau covered with rocky remains. The eastern summit also consists of mica and mica-grant slates, which form a conical mountain (Borisevich 1968, Geology of the USSR 1969). Here, a weather station is situated.

Climatic conditions

The meteorological station at the top of the DTM plateau (Taganay-Gora, 55° 22'N, 59° 55'E, 1102 m a.s.l.) regularly recorded weather conditions from 1932 to 2001. A meteorological summary reports an average annual temperature of -1.9°C, an average January temperature of -15.4°C and July is +12.3°C; the absolute minimum is -33.6°C, the absolute maximum temperature is +26.6°C. Negative temperatures are recorded in the first week of October until the last week of April. The sum of positive temperatures above 10°C is from 800 to 950, the duration of the frost-free period is about 100 days. Late spring and early autumn frosts occur quite often, frosts end in the first half of June, and begin in early September, and therefore, the duration of the growing periods ranges from 70 to 90 days.

Figure 1: Study area.

The local climate is affected by stoppage and significant transformation of moist Atlantic air masses and cyclones. Average annual precipitation is 1000 mm with 320 mm of annual evaporation recorded. Up to 70% of precipitation falls during summer months, with a maximum in July. Stable snow cover lasts 200 days, air humidity ranges from 64 to 84%, and the average depth of soil freezing is 66 cm. Snowstorms are frequent during winter(132 days) and fog conditions can be observed throughout the year (240 days per year).The area is predominantly affected by west and south-west wind directions. The average annual wind speed at the ridge reaches 10.3 m/s, and the maximum recorded speed is more than 50 m/s. (Agroklimaticheskiy spravochnik 1960).

Upper tree-line definition

At the research site, the upper tree-line is a zone between single or multistem trees and the sparse mountain forests below. This area is a narrow strip of relatively homogeneous growth conditions. There are single-standing trees and/or multistem individuals, which form micro-groups of trees originating from one root. Above this zone, tree stems do not occur and shrubs predominate (Schroeter 1926, Gorchakovsky & Shiyatov 1985). Crown density does not exceed 0.2. In some cases, the upper tree-line is broad coinciding with an upper ecotone level, while in other settings the tree-line can be a narrow sharply delineated line.

Allocation of borders

The upper tree-line of each of the three summits of the DTM was analyzed using both remotely-sensed images and actual maps (Google Earth, SASPlanet). Subsequent field reconnaissance of the tops was completed to identify the most obvious environmental drivers influencing the tree-line position during last decades.

Collection of samples

The maximum tree-line elevation on the DTM is 1089 m a.s.l. Representative sites were selected at each ecological type of upper tree-line, where cores were collected from Siberian spruce (*Picea obovata* Ledeb.) at 0.3-0.5 m height. Samples were gathered at the uppermost edge of the tree-lines and typical morphometric characteristics of the trees in the selected sites were described. At each site 30-50 cores were taken from single standing trees or one - two of outer stems of multistem individuals. Tree height and stem diameter at breast height were measured, and the type of crown was described as a flag-shaped or a double crown (lower part of crown is near ground at 0.5 m height and the second upper part is separated from the lower part by 0.5-0.8 m by a trunk without branches).

Sample handling

Samples of wood were polished and measured using the TSAP software and cross-dated using COFECHA and frost rings, which narrow rings are forming in response to frost events in the research area. The number of samples was reduced by removing samples with the lowest interseries correlation to form tree-ring chronologies with greater sensitivity and intersample correlation. In this process, at least 10 tree-ring series were chosen from each type of tree-line with the highest correlation coefficients. Generalized tree-ring chronologies were then constructed to reveal differences in tree growth dynamics on ecological tree-lines.

Results & Discusson

The size of the treeless central plateau of the DTM is 0.4x0.4 km. We can identify and allocate four main limiting environmental drivers: temperature, wind, snow and lack of soil. Four main ecological types of the upper tree-lines are proposed for the DTM.

Types of tree-lines

1. Thermal line

Strictly controlled by temperature, the thermal tree-line is located at the highest elevation on the south-western exposure of the summit. Consequently, environmental conditions are very favourable for tree growth. The thermal tree-line is characterized by a gentle slope of ~8-10 degrees forming an ecotone (a smooth transition from closed forest to separately standing single trees) (Table 1). Single trees have often a symmetrical round-shape crown sometimes double crowns were be noted. Multistem forms were observed often. The flag-shaped crowns are absent indicating little influence from wind influence likely provided by the DTM ridge (Fig. 2a). The site has a flowing type of water regime in spring; a lot of water mass form during spring snowmelt, but water flows away very fast and during the growth period soil moisture is normal. Generally, trees are *Anemonas trumbiarmiensis* young; the average age of the selected models was about 20 years at 0.3-0.5 m height (Table 2). There is abundant germination and regeneration of spruce on the slope; up to 50 spruce seedlings up to 50 cm height can be found with in 20 m^2. The young generation of spruce mixes with infrequent birch up to 70 cm height. The herbaceouslayer includes *Vaccinium uliginosum, Empetrum nigrum* sp. *hermophroditum, Aconogonon alpinum, Polygonum bistorta, Anemonas trumbiarmiensis, Arctrous alpina, Cladonia* and *Cetraria* lichens.

Table 1: Physical characteristics of ecological tree-line types on study sites.

Tree-line	Elevation, a.s.l., m	Exposure	Slope angle upper/below tree-line (degrees)	Transition tundra/closed forest
Thermal	1096	SW	8/10	ecotone
Wind	1077	S	13/18	mixed
Snow	1081	NE	30/4	sharp
Edaphic	1001	NW	52/15	sharp

2. Wind line

The wind tree-line is located on the southern slope of DTM. The absence of natural topographic protective barriers yield strong and persistent wind activity. Despite the gentle slope angle and developed soil above the wind tree-line, the trees grow lower here than at the thermal tree-line. The closed forest stands form a sharp tree-line delineating the wind-blown section of the slope, and upslope from the tree-line infrequent, separately-standing single trees with the flag-shaped crown are present (Fig. 2b). The flag-shaped crowns are orientated up the slope from the south to the north. Consequently, on the DTM southerly winds limit tree growth despite the high frequency of western and south-western wind activity. The flag-shape of the tree crown is formed due to the drying effect of the wind, and subsequent deleterious insect activity on the windward side. Winter snow ablation can cause insect mortality, which is observed above the snow pack level. Dying branches and increased wind loads form eccentric stems. Single flag crowned and multistem spruces are growing on the DTM, but prostrate forms of spruce are not present, suggesting strong but not catastrophic wind impact. The average age of spruce is about 20 years. Regeneration of spruce is weak, the several birches are appeared. The composition of the herbaceous layer indicates a dry soil moisture regime and is dominated by wind-hardy species including *Anemonas trumbiarmiensis*, *Festuca ovina*, and other cereals, *Aconogonon alpinum*, *Arctrous alpina, Cladonia* and *Cetraria* lichens.

Table 2: Tree characteristics at ecological tree-lines. Crown/stem deformation: 2 – double crown, F – flag-shape crown, B – bended stem.

Tree-line	Height, m	Diameter BH, cm	Mean age at 0.5 m, years	Crown cover	Multystems trees	Crown/stem deformation
Thermal	2	3	18	0.2	+	2
Wind	2	5	20	0.1	-	2, F
Snow	0.5	3	25	0.1	+	B
Edaphic	6	10	74	0.5	-	-

3. Snow line

The snow tree-line has a very short segment on the north-east slope of the western top of DTM In Fig. 2c the wind tree-line is outlined on the background of the photo, the thermal tree-line ecotone on the south-west exposure is visible, and the snow tree-line is at the foreground on the north-east slope. Prior to the 1980s, a snowfield and small glacier were found at the study site, however, the contemporary landscape is characterized by a delay of the beginning of the vegetation period of 7-10 days (according to plant phenophases here). Snow accumulation and snowmelt rate depend on several drivers. Firstly, winter snowstorms transfer snow from the upper part of the western and central tops contributing to snow accumulation during the cold period. Second, the north-eastern exposure receives little direct solar radiation delaying the spring snowmelt. As a result, this tree-line has a clearly defined form and border. The site is waterlogged due to abundant snow and slow melting. Reproduction of spruce is weak; trees are stocky, up to 0.8 m height, with dead lower parts of the crown, and bends and thickening of the stem at the base. The trees have dead lower branches and the living part of crown has very dense branches. This dense crown indicates a slow rate of growth during the growth period. At the base of the stem, all trees have a stem thickening or stem

bend, indicating the frequent dying off of the lateral buds, branches and axial shoot. Most trees are multistems. The samples collected at 0.2-0.3 m height (above stem thickness) have around 25 tree-rings on average. However, the actual biological age of these spruces is longer, and the vertical stems started to grow during the last 25-30 years. An herbaceous layer is dominated by *Empetrum nigrum* sp. *hermophroditum, Arctrous alpine, Aconogonon alpinum, Juncus trifidus, Anemonas trumbiarmiensis, Polypodiophyta.*

4. Edaphic line

The most widespread type of an upper tree-line on the DTM is the edaphic line. The extension upwards of the tree-line to the mountain top is limited by large disorganized piles of rocks and large stone fragments, forming steep slopes. This tree-line is confined to the northern and eastern slopes, with slope steepness exceeding 30° primarily influencing its position. As a result, the tree-line is situated lower than the others, and has the sharp outlined tree distribution. The soil above the tree-line is usually absent or poorly developed limiting tree ascent by the absence of a grow substrate. At the study site tall trees (up to 8 m height) form a closed forest stand, with birch, dog rose and rowan in the undergrowth. The average age of the trees collected was 74 years, and the oldest individual is 152 years old. The regeneration of spruce is weak due to high competition. An herbal layer consists of blueberries, various cereals, bulrush, ferns and green mosses (*Pleurocium* sp.). The soil has flowing type of moisture.

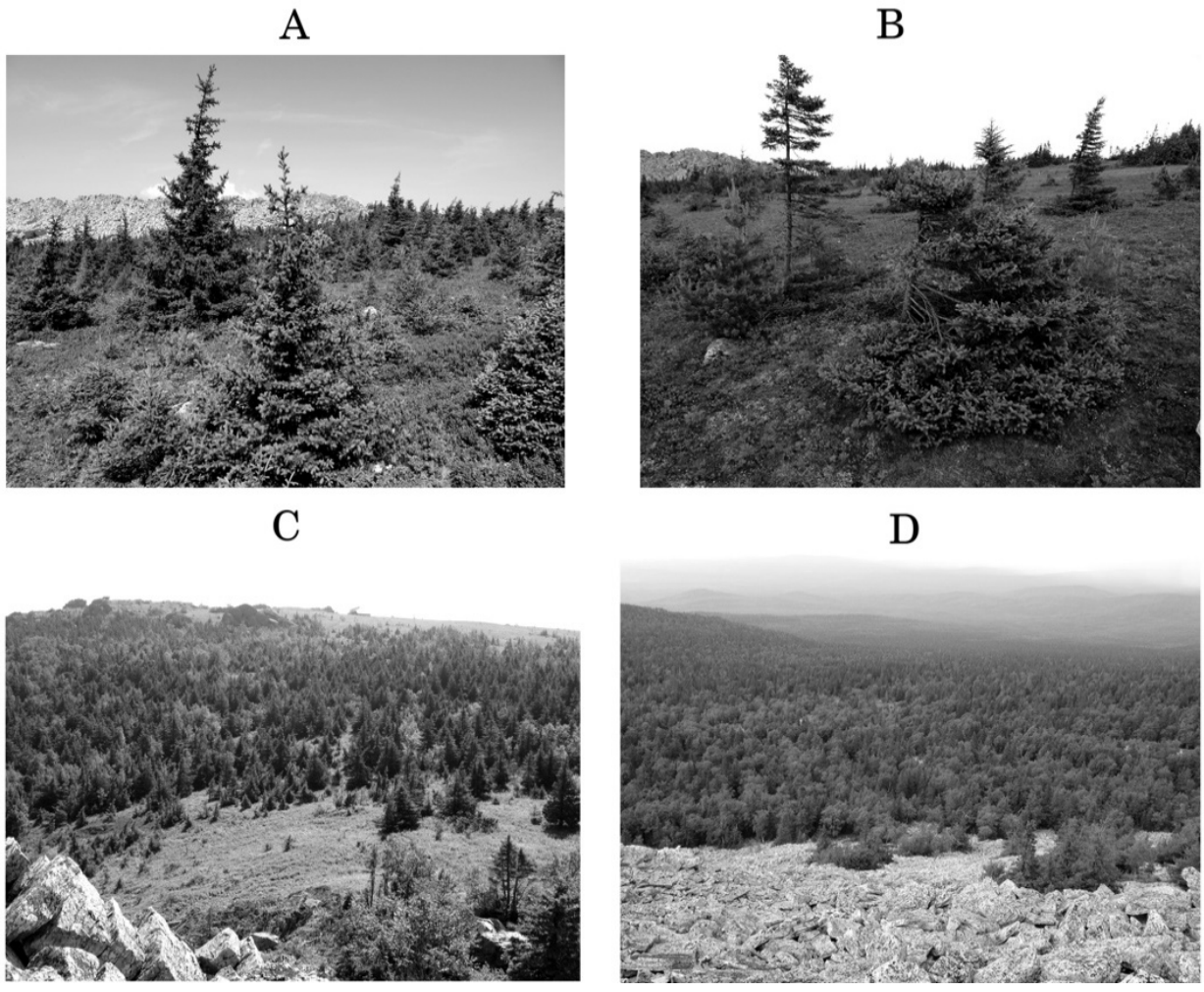

Figure 2: Main type of ecological tree-lines at the DTM A – thermal, B – wind, C – snow, D – edaphic.

Tree-line ratio

Based on the data revealed during the field inspection of different growing conditions, a schematic chart of the different ecological types of upper tree-lines at the DTM was completed (Fig. 3). The most widespread and common type of tree-line is edaphic. It extends 30% of total length of the spruce tree-lines on the central plateau top and 95% of the total tree-line length on the western top. These differences of edaphic tree-line length depend on slope steepness.

The thermal tree-line has up to 45% of the length of the central plateau, and occurs at the south-western and north-western exposures. Favourable grow conditions are created by relief and exposure. The western top shelters the area for west and south-west winds, the south-western exposure receives more solar radiation, and the north-west top has a lot of snow during winter and ample water availability during summer. These growing conditions facilitate upslope habitat for trees.

The wind tree-line covers 25% of the total length of central plateau as is located on the gentle slopes, but because of strong winds the tree crowns have flag-shaped forms.

The shortest tree-line in the study region is the snow upper tree-line, which is located along the snowfields and snow packs sites covering up to 5% of the general length of tree-line on the western summit. Historically this tree-line was not long and large. Recent climate changes including increased air temperature (Moiseev et al. 2016) decrease the snow tree-line gradually with previously tree-free area becoming overgrown with spruce, birch and different shrubs (Fig. 3).

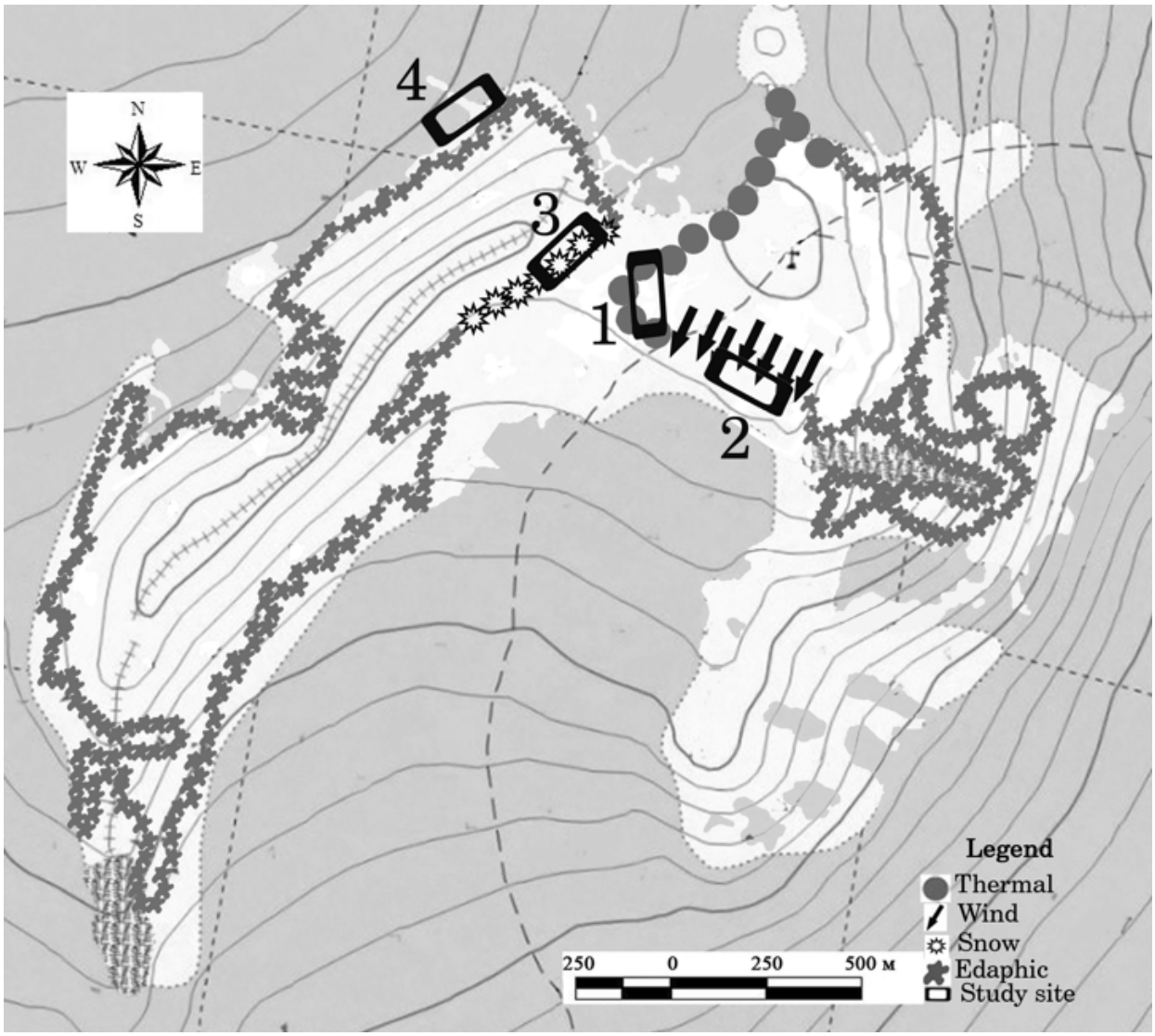

Figure 3: Outline of tree-lines on DTM. Grey filling – tree-line in the 50s of the 20th century.

Tree-ring chronologies of different types of tree-lines

The 152-year edaphic tree-line chronology represents the longest tree-ring chronology, while the wind tree-ring chronology spans 25. The narrowest mean annual ring width is marked on the thermal tree-line and the widest width is on the wind tree-line (60% wider than the thermal tree-line).Wide rings of the wind tree-line chronology are associated with the eccentricity of the tree stems. The widest rings are found on the wind and snow boundaries (over 3 mm wide), and on thermal and edaphic tree-line it is less than 3 mm (Table 3). Annual growth rates increased during last ten years on thermal, wind and snow tree-lines, and decreased on edaphic line (Fig.4).
Interseries correlation is the main indicator of congruence between individual time series. The highest correlation between the series is recorded at the thermal tree-line, with lower correlation coefficients calculated from chronologies collected at the thermal and edaphic tree-lines. Shiyatov (1986) also noted low correlation coefficients in tree-ring chronologies collected from edaphic valley sites (r = 0.33).

Table 3: Tree-ring chronologies on different upper tree-lines.

Tree-line	N series total /chronologies	Time span	Mean tree-ring width, mm	Maximal tree-ring width, mm	Sensitivity	Interseries correlation
Thermal	50/20	1985-2014	0.44	2.88	0.35	0.59
Wind	50/18	1988-2014	0.75	3.08	0.34	0.47
Snow	25/13	1980-2014	0.47	3.09	0.43	0.42
Edaphic	50/17	1865-2014	0.54	2.91	0.25	0.34

The sensitivity of tree-ring series indicates harsh growing conditions. An individual series is sensitive if the sensitivity coefficient is greater than 0.3. The highest sensitivity of the tree-ring series was found at the snow upper tree-line, the lowest is at the edaphic line. In the Southern Urals sensitivity coefficients at the upper tree-line are generally low reaching only 0.31 (Shiyatov 1986). Our data show that the values of sensitivity coefficients are high, especially in the harsh conditions of extremely short growing period at the snow tree-line. Here the values of the sensitivity coefficient reach the Subpolar and Polar Urals values (Shiyatov 1986).
Correlation coefficients between generalized tree-ring chronologies from different ecological types are not high. The closest relation was statistically obtained between the wind and thermal tree-line chronology (r = 0.54, N=30). These two chronologies were developed from tree cores collected from trees growing proximally on a similar slope exposure (south-west and south), similar elevation and approximately the same time of vertical tree stem appearance (at 0.5 m stem height).

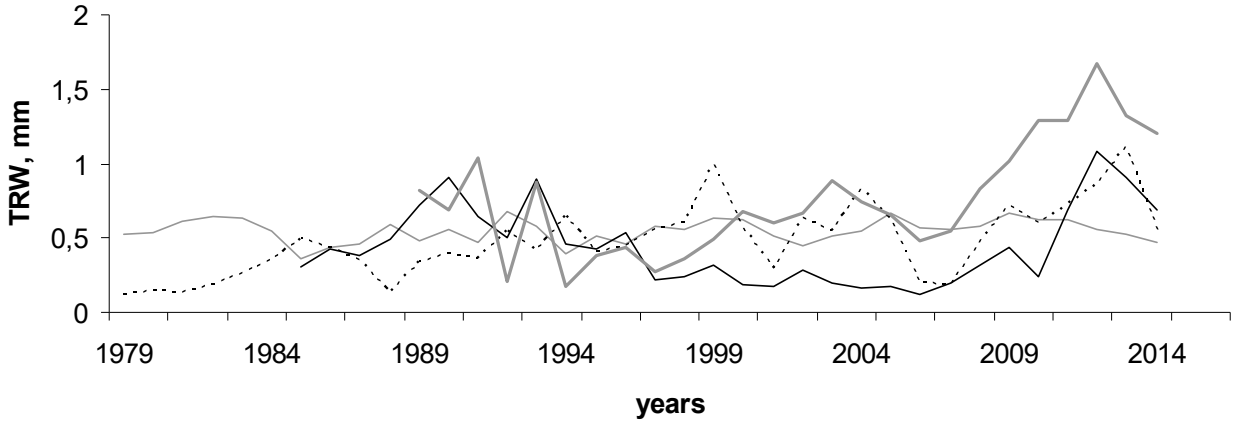

Figure 4: Generalized tree-ring chronologies. Black line – thermal, thick grey line – wind, dotted line – snow, thin grey line – edaphic upper tree-line.

Synchronicity between tree-ring chronologies from different tree-lines changes from very high until middle values. The thermal and wind tree-line chronologies are most synchronous with 95% of similarity, while minimum synchronicity is exhibited between the snow and other types of tree-lines (74% of similarity). The edaphic tree-line has intermediate value (81% of similarity). Thus, in a very small area the trees have different growth dynamics connected with different environmental drivers.

Conclusion

Preliminary estimates of ecological upper tree-line types in the Southern Urals are presented in this study. Differences between the tree-lines based on elevation, slope exposure, wind direction and level of soil moisture are shown. These conditions lead to various tree morphology and different dynamics of annual growth. In future research, a more precise definition of the limiting drivers is required.

Acknowledgements

This work was supported by the State Contract of the Institute of Plant and Animal Ecology, UB RAS and Russian Foundation of Basic Research (grant No 15-04-04933).

References

Agroklimaticheskiy spravochnik po Chelyabinskoy oblasti (1960): Leningrad: Hydrometeoizdat. 156. (in Russian).

Borisevich, D.V. (1968): Relef i geologicheskoe stroenie. In: Komar I.V., Chikishev A.G. (Ed.) Ural i Priurale. M.: 19-81. (in Russian).

Danby, R.K., Hik, D.S. (2007): Variability, contingency and rapid change in recent subarctic alpine tree line dynamics*. Journal of Ecology*:(95) 352–363.

Geologiya SSSR. T XII. Permskaya, Sverdlovskaya, Chelyabinskaya i Kurganskaya oblasti. Chast 1. Geologicheskoe opisanie. Kniga 1. (1969): M: Kniga po trebovaniyu. 777. (in Russian).

Gorchakovskiy, P.L., Shiyatov, S.G. (1985):Fitoindikatsiya usloviy sredy i prirodnyih protsessov v vysokogoryah. M.: Nauka. 208. (in Russian).

Kullman, L., Öberg, L. (2009): Post-Little Ice Age tree line rise and climate warming in the Swedish Scandes: a landscape ecological perspective. *Journal of Ecology*: (97) 415–429.

Mazepa, V.S. (2005): Stand density in the last millennium at the upper tree-line ecotone in the Polar Ural Mountains. *Canadian Journal of Forest Research*: 35(9) 2082-2091.

Moiseev,P.A., Bartyish, A.A., Nagimov, Z.Ya. (2010): Izmeneniya klimata i dinamika drevostoev na verhnem predele ih proizrastaniya v gorah Severnogo Urala. *Russian Journal of Ecology*: (6) 432-443. (in Russian).

Moiseev, P.A., Shiyatov, S.G., Grigoriev, A.A. (2016): Klimatogennaya dinamika drevesnoy rastitelnosti na verhnem predele ee rasprostraneniya na hrebte Bolshoy Taganay za poslednee stoletie. Ekaterinburg. 136. (in Russian).

Shiyatov, S.G. (1986): Dendrochronologia verhney granisy lesa na Urale. M.:Nauka: 136.(in Russian).

Schroeter, C. (1926): Das Pflanzenleben der Alpen: Eine Schilderung der Hochgebirgsflora. Zurich: Verl. von Albert Raustein. 1288.

Remote-sensing data are closely related to growth information in tree-ring index chronologies

J. Schröder[1] & M. Körner[2]

[1] Landeskompetenzzentrum Forst Eberswalde, Alfred-Möller-Straße 1, 16225 Eberswalde, Germany
[2] Staatsbetrieb Sachsenforst, Bonnewitzer Str. 34, 01796 Pirna OT Graupa, Germany
E-mail: jens.schroeder@lfb.brandenburg.de

Introduction

Statistical simulation programs widely used in forest growth and yield science usually estimate the development of trees and stands in time steps of five years as a result of the data base used for their calibration (Nagel et al. 2006, Pretzsch 2009). Further differentiation into annual estimations is only possible by dividing the derived estimates into smaller units of equal value. The inter-annual variability in the environmental factors that control biomass productivity and timber increment is not adequately reflected by this approach. In a forest growth context, diameter at breast height (dbh) is commonly regarded as a sufficiently representative indicator of varying environmental conditions (Pretzsch 2001). Its development over time can easily be reconstructed and analyzed by means of borer cores and the derived tree-ring width time series (Schröder 2015). Individual-tree and stand mean dbh also belong to the central parameters in forest growth and yield simulations. For flexible, annual estimations without tree-ring width information these simulations need independent and reliable data on environmental conditions that are closely related to annual increment and therefore allow modifications of average dbh projections according to how favourable the specific year's climate had been for growth.

Remote sensing technologies provide a wide array of data representing the status of and the variability in the activity of different types of vegetation (Kaufmann et al. 2008, Bhuyan et al. 2017). Optical sensors capture radiation in different wavelength and frequency bands reflected from the earth. The intensities in these bands result from the photosynthetic activity of the plants: Areas with photosynthetically active vegetation absorb much more radiation in the red portion of the electromagnetic spectrum than areas with little or no active vegetation. In contrast, absorption of near infrared (NIR) radiation is low for active surface types as well as for surfaces without vegetation. The Normalized Difference Vegetation Index (NDVI; Tucker 1979) relates the difference between NIR and red radiation to the sum of both parameters. Although the total potential range is between -1 and +1, data services usually provide NDVI values with $0 \leq NDVI \leq 1$ (or $0 \leq NDVI \leq 10{,}000$ to avoid decimal digits). The larger the value, the greater the "gap" between red and NIR, and thus the more intense the photosynthetic activity of the respective vegetation.

The interrelations between NDVI and tree rings in their role as comprehensive indicators of variance in forest and tree growth have been targeted by a wide range of studies. Kaufmann et al. (2008) analyzed the effects of tree-ring growth on NDVI and vice versa under the influence of varying climate. Bhuyan et al. (2017) explored the potential of remote sensing data on different spatial scales including NDVI measures to estimate tree-ring growth and leaf activity for 69 forest sites in the northern hemisphere. Wang et al. (2004) investigated the relations between the annual variation in productivity of North American forests "as represented by tree ring width residuals, diameter increase, and seed and foliage production" to single and integrated NDVI detected for the respective stands. They found significant correlations and concluded that the radiation index can be a valid indicator for varying increment in forest stands. Their results were the basis for preliminary studies of the connections between NDVI and tree-ring width on trial plots in the state of Brandenburg, Germany. Our paper is based on the findings of these studies and expands them by a comprehensive methodological approach to explore and model the statistical significance of the relations between NDVI and tree-ring width.

Data and methods

The data used in the following analyses were collected in the forest districts "Heegermühle" and "Spechthausen" located in the north of the German state of Brandenburg (Fig. 1). Three temporary trial plots were established in pure, even-aged stands of Scots pine (*Pinus sylvestris* L.) which is the dominating tree species in the region and occupies around 75% of all forest land in the state. The respective stands were chosen in different age classes to capture the most important phases in the species' life cycle. Basic trial plot data are given in table 1 below.

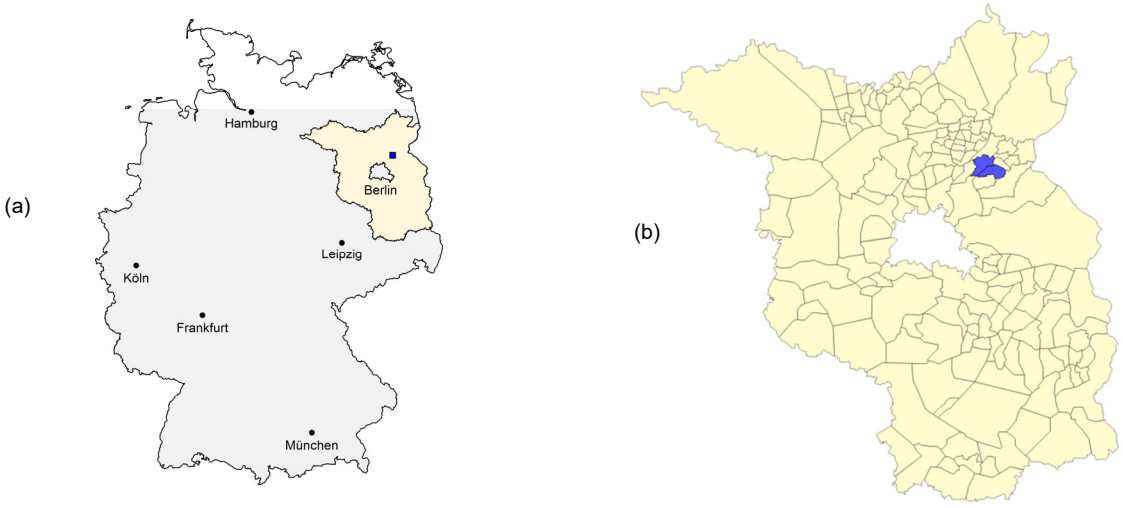

Figure 1: Location of the study area and the trial plots in Germany (a) and in the State of Brandenburg (b). Figure 1b shows the forest districts Heegermühle and Spechthausen (blue).

Table 1: Basic data of the three trial plots (reference: 01.01.2015)

plot	district/address	A [m²]	age	N/ha	dg (dbhs) [cm]	hg (hs) [m]	BA [m²/ha]
1	HE 182 a2	300	44	2.633	13,6 (6,8-24,3)	15,1 (10,3-18,3)	38,1
2	SP 81 b3	400	69	975	21,6 (11,2-34,2)	21,1 (14,9-24,2)	35,6
3	HE 141 a2	500	98	380	28,1 (21,3-37,4)	22,7 (18,2-26,5)	23,5

with HE = Heegermühle, SP = Spechthausen, A = plot area, N/ha = tree number per hectare, dg = dbh of mean basal area tree, dbhs = min.-max. dbh on plot, hg = value of height-diameter function for dbh, hs = min.-max. height on plot, BA = stand basal area per hectare

Tree-ring measurements predominantly allow the reconstruction of radial increment time series, usually exluding the bark fraction of a tree's dbh. Our study accordingly focused on this increment level instead of derived basal area or volume increments which would relate more closely to the scale of biomass productivity (Pretzsch 2009). We did, however, include bark thickness by setting the individual dbh outside bark as a reference for correction of the measured tree-ring width (TRW) series: To reconstruct individual radial growth two cores were extracted by using manual increment borers from 20 trees per plot at breast height (1.3m). From the individual TRW measurements we derived tree-specific time series for radial increment by averaging and standardizing the TRW time series to the radius at breast height without bark (Beck 2007). TRW series were complemented by tree-ring index time series (TRI) varying around a mean of 1. These TRI series reflect predominantly short-term, i.e. annual influences on tree growth (Schröder 2015). The 20 samples per plot were taken from 10 comparatively large and 10 comparatively small trees to allow

investigations into possible effects of a tree's social status on the relations between increments and NDVI. As a result of this approach nine separate groups (or sub-samples) were created: three sample plots each with (i) the total of 20 trees, (ii) 10 "dominant" trees, and (iii) 10 "suppressed" trees. All individual time series were tested for conformity with a sub-sample-related average dbh (diameter at breast height) growth course (Beck 2007), and trees obviously differing from this average development were excluded from the respective group before deriving sub-sample-specific (arithmetic) mean TRI time series. For all steps in processing TRW data into TRI we applied the `dplR` package within the statistical software `R` (Bunn 2008, Bunn et al. 2015, R Core Team 2015). The program TriCycle was used to obtain necessary file formats from the measured TRW (Brewer 2011).
Sub-sample TRI series were correlated to time series of remote sensing data obtained from the website of the NASA Terra satellite system. Terra satellites transport the MODIS sensor which has been capturing radiation data since February 2000. NDVI data are available free of charge in the MOD13Q1 product which processes the NIR radiation and the radiation in the visible range of wavelengths (VIS), composed mainly by the red partition, as reflected from the earth (see Equation 1; NASA 2016).

$$NDVI = (NIR — VIS) / (NIR + VIS) \quad \text{Eq. 1}$$

The NDVI in the MOD13Q1 product has a spatial resolution of 250×250m and is available in a temporal resolution of 16 days which results in 23 values (stored in individual files) in the interval January 1 to December 19. Their position within the year is indicated by the "day of year" (DOY) property of the respective value that represents the mean day of the 16-day period the particular image was captured in. Data may be downloaded in tiles covering an area of 10×10 degrees (referring to a 360-degrees coverage of the earth's total surface; NASA 2016a). From these large tiles a smaller area was cut of a size of 68×50 pixels, i.e. 17×12.5km = 231.5km² matching the region were the trial plots were located. Our analyses involved increment data ending in 2014 so we used NDVI information for the years 2001 to 2014. For the preliminary data processing and extraction of pixel information the `R` packages `raster`, `rgdal`, `shapefiles`, and `sp` were applied (Bivand et al. 2015, Hijmans 2015, Pebesma and Bivand 2015, Stabler 2013). NDVI time series for the three plots were obtained from the pixels that cover the coordinates of the geometric center of the respective forest stand. According to NASA (2016a) the "valid range" is identical with the interval between -0.2 and +1.0 but figures in the MODIS files are multiplied by 10^4 to avoid problems related to decimal digits (see also Tucker 1979). Raw NDVI data were checked for outliers that can be caused by meteorological disturbances such as clouds, fogs, rain etc.: Values between DOY 49 and DOY 305 that differed by more than 30% from the average of their immediate temporal neighbors were replaced by this average. Fig. 2 shows an example for the resulting "smoothed" series that were eventually used for correlation analyses.

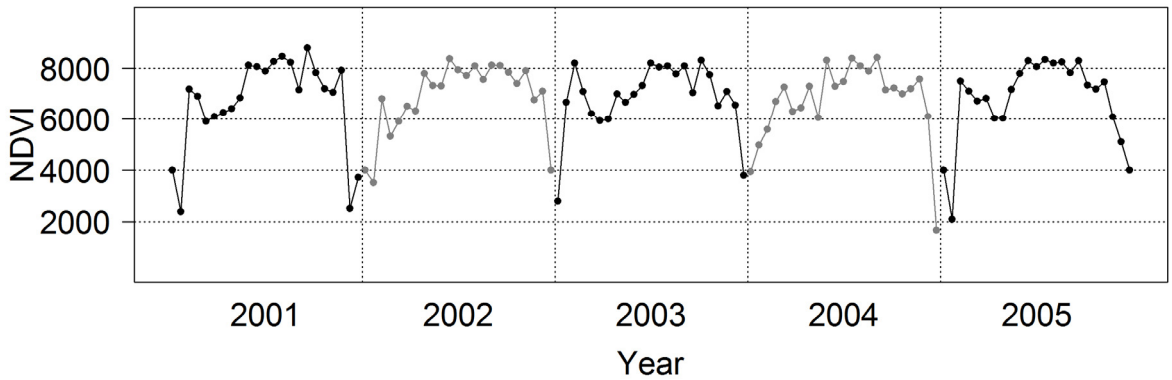

Fig. 2: Smoothed NDVI series of the years 2001-2005 for plot 2 (see tab. 1 for plot properties)

The subsequent analyses were aimed at identifying those DOY whose NDVI information was most closely correlated to the trial plots' TRI time series. We tested not only individual DOY but also the mean values of series of DOY with all possible lengths at all positions within the year including the longest possible series starting on DOY 1 and ending on DOY 353. Consequently there were 231 possible single DOY and DOY series per year. The interval to search for maximal correlations had a minimal length of five years in the period 2001 (first year of complete data availability) to 2014. This approach resulted in a total of 55 "time windows" starting from ten five-year intervals that begin in 2001 to 2010, respectively, to the maximum window of 14 years (2001-2014). Input data included not only the NDVI of the three central pixels that cover the trial plots but also the mean values for 3×3 clusters (composed of the central points and their immediate neighbors) and the mean of all three 3×3 clusters to capture the "average" NDVI course in the region.
To study the relations between NDVI and tree rings, we focused on TRI because this variable better represents the annual variability of increment due to its stationary mean and the increased relative sensitivity of the series (Schröder 2015). Fig. 3 demonstrates the transformation from TRW time series into mean curves of TRI for all trees on plot 2 and for the sub-samples of dominant and suppressed trees.

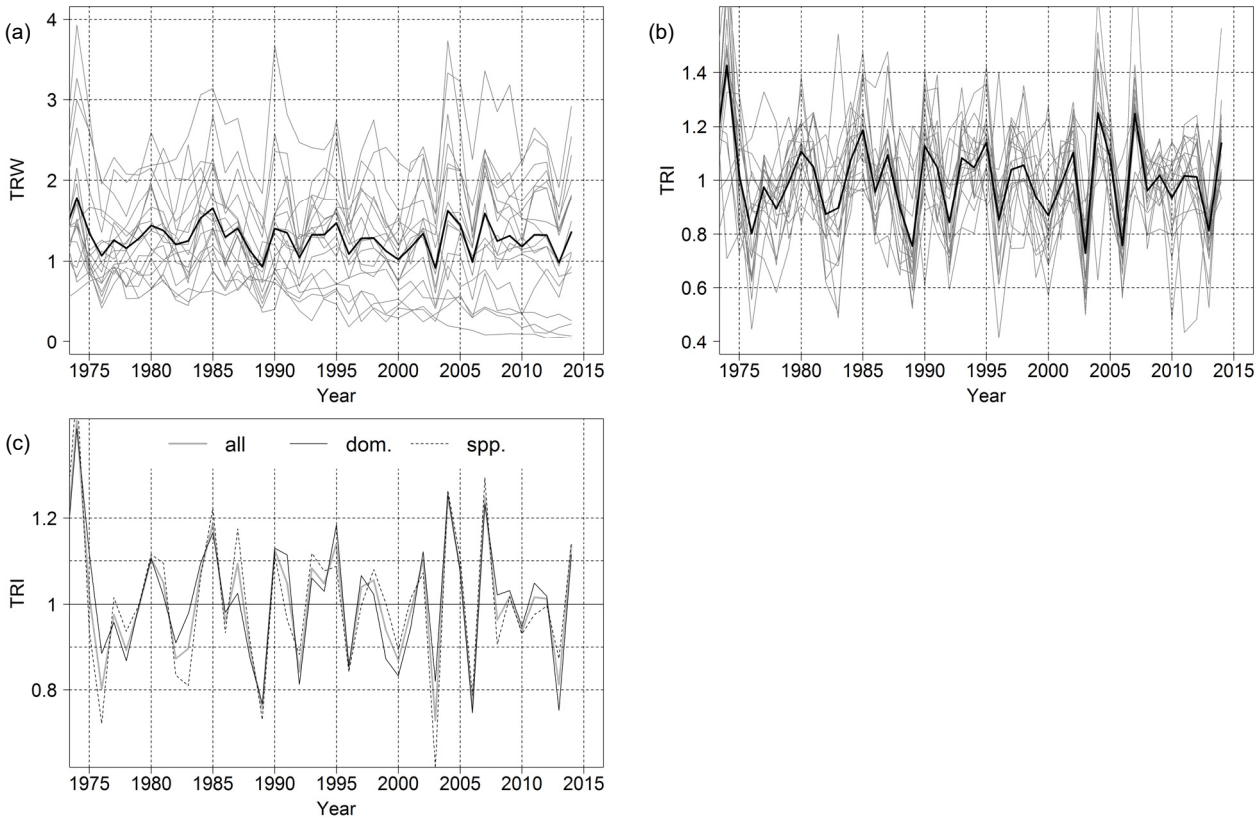

Figure 3: Transformation of individual TRW time series (a) into TRI series (b) for trees on plot 2 (n=20). Blue lines in (a) and (b) represent single trees, black bold lines the arithmetic means. Diagram (c) shows sub-sample average time series for all 20 trees ("all"), for dominant ("dom."), and for suppressed trees ("spp.").

Correlation analyses were done for the nine TRI time series resulting from the three sub-samples from three plots. The strength of the relations between TRI and NDVI was assessed by Pearson's correlation coefficient *r* together with the statistical significance indicator *p*. The necessary algorithms were programmed in R with the ordered results stored in a csv-format file. Each line in this file contains the *r* and the *p* of an individual correlation, the begin and the end of the respective yearly NDVI window (as DOY), the number of images combined in this series, the period (years), the type of pixel information (single, cluster, or all together), and the TRI sub-sample involved into

the particular analysis. The following section presents selected results of the chosen methodological approach.

Results

Correlations between TRI and NDVI time series are in many cases very close and highly significant. The main influence on these dependencies was executed by the position of the involved DOY interval within a year and the length of this interval. Although the majority of correlations showed positive *r* values there were also a number of significant negative correlations (Fig. 4a). The mean of the significant positive correlations (which are biologically much more plausible) exhibits a decreasing trend with the number of years selected from the total reference period (Fig. 4b). The temporal position of the analyzed intervals within the period 2001-2014 had no relevant effect on the mean correlation coefficients, so there is no individual period in this time that would have been more suitable than other periods for representing the general relations between NDVI and increment rate.

Before NDVI time series can be used to model TRI it has to be resolved which reference interval (DOY span) should be employed. Additionally we wanted to clarify the potential differences in the relations caused by age or social status of the trees by comparing the results for the individual plots and sub-samples. Dominant trees usually depict climatic effects in their inter-annual increment variability more clearly than suppressed trees whose tight competition situation tends to disturb climatic signals in TRI time series (Schröder 2015). However, comparisons of average TRI time series per sub-sample for the different plots have already provided first hints towards a uniformity of growth reactions irrespective of the social status of the sampled trees (Fig. 3c). The distributions of significant positive correlation coefficients per sub-sample and per plot further strengthened the conclusion that there are no differences in the relations of TRI to NDVI between the selected social groups (Fig. 5a).

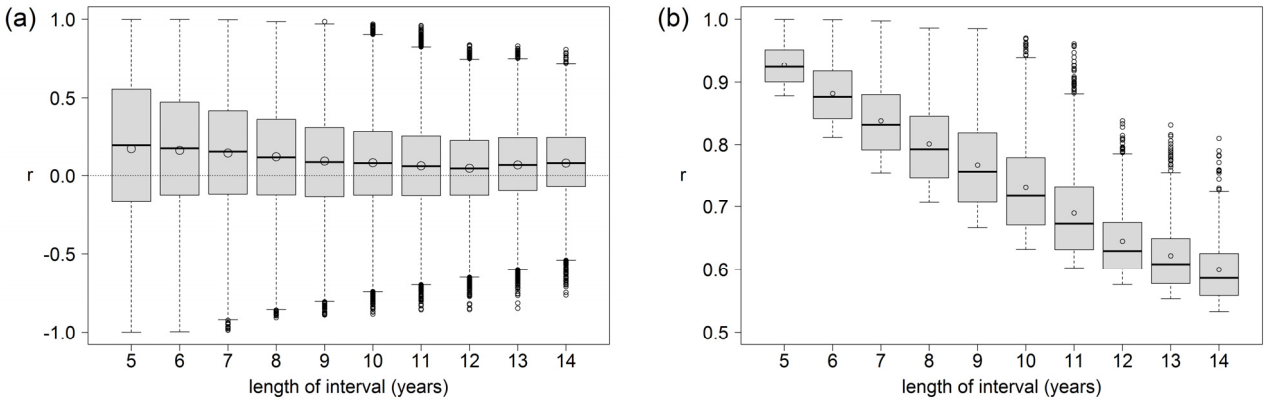

Figure 4: Distribution of correlation coefficients (r) between NDVI and TRI for all plots and sub-samples over length of reference interval (a). Hollow dots in boxes represent the arithmetic mean. Figure (b): distribution of r for the significant positive correlations.

The source of NDVI information (single pixels, 3×3-pixel groups, or mean over the three pixel groups) influences the number (n) and the strength (r) of correlations with TRI (Fig. 5b). The diagram shows the distributions of all significant positive r derived for time series with a length of 14 years. While plots 1 and 3 had much more significant correlations when pixel-group NDVI series ("...-9") were employed, plot 2 showed a smaller number and a lower median for this data source compared to the data derived from single pixels ("...-1") covering the coordinates of the plot center. NDVI data over 14 years calculated as arithmetic mean of all 3×3-pixel groups were significantly correlated with TRI only for the dominant trees on plot 3 and for all sub-samples on plot 2.

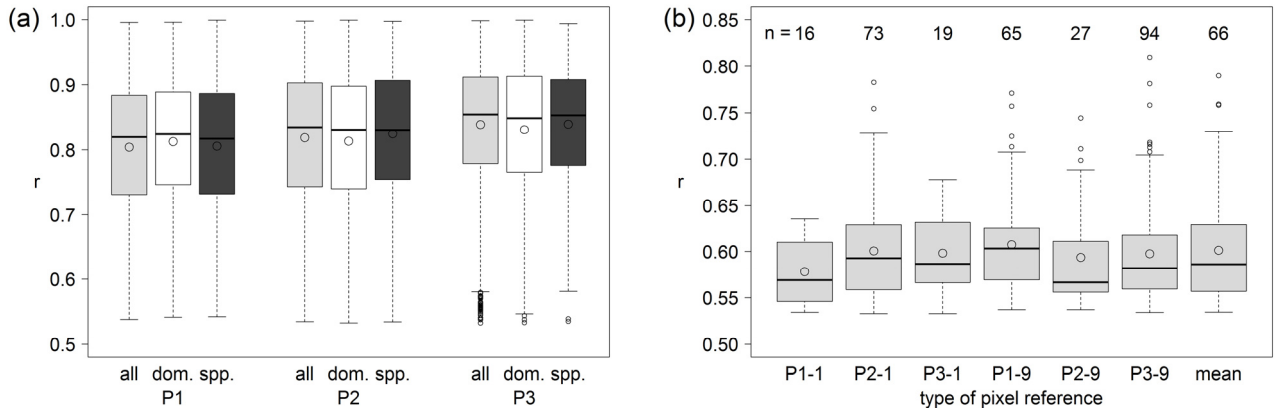

Figure 5: Distribution of significant positive correlation coefficients (r) between NDVI and TRI for all plots separately for the social groups (a), "all" = all trees of a plot, "dom" = dominant, "spp" = suppressed; "P1"-"P3" = plot 1 to plot 3. (b): Distribution of r for time series of 14 years according to the pixel reference used for NDVI calculation (see text), "n" indicates the number of significant positive correlations per sub-group.

Correlations vary not only according to the employed TRI and NDVI data sources but also in relation to the calendar position of the respective temporal windows, i.e. the DOY of their begin and end. Maximum coefficients for correlations covering the total available interval 2001-2014 result for temporal sequences of images beginning on DOY 65 (March 3rd) and on DOY 225 (September 12) (see Fig. 6a). In a first approach we focused on DOY 65 that marks more or less the start of the growth period for Scots pine. Among the image series that could be used to derive NDVI averages the most promising were those that had a length of two to six successive images because they showed reliably strong correlations with TRI. Within this group, aggregates (mean values) of four images (DOY 65 to DOY 113, i.e. 06.03.-23.04.) yielded the highest absolute *r* values (Fig. 6b).

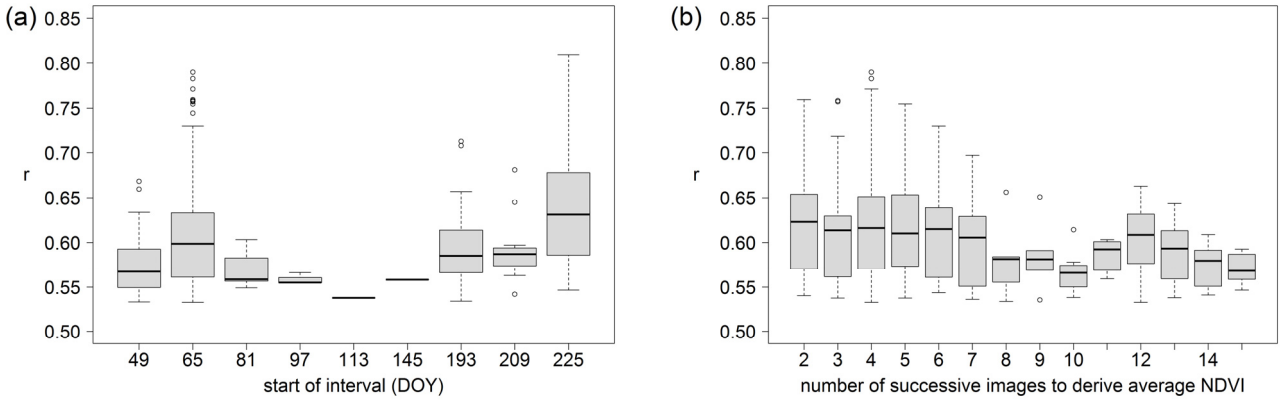

Figure 6: Distribution of positive correlation coefficients (r) between NDVI and TRI for all plots over DOY of the first image of the analyzed series (a). The x-axis shows only those DOY for which significant r could be derived. (b): Distribution of r over number of successive NDVI image aggregates starting on DOY 65.

Based on the correlation analyses we developed a simple linear model to estimate TRI from the most suitable NDVI aggregates. The arithmetic mean of the four images from DOY 65 to 113 (06.03. to 23.04., see above) over all 3×9 pixels was used as independent variable; the function is calibrated to model the TRI series of dominant trees on plot 2. Because NDVI data of the year 2000 start on DOY 49, this year could also be used in model development. Figure 7 shows the time series of annual TRI and the selected NDVI information (a) and compares the real TRI with the modeled values of the linear function (b).

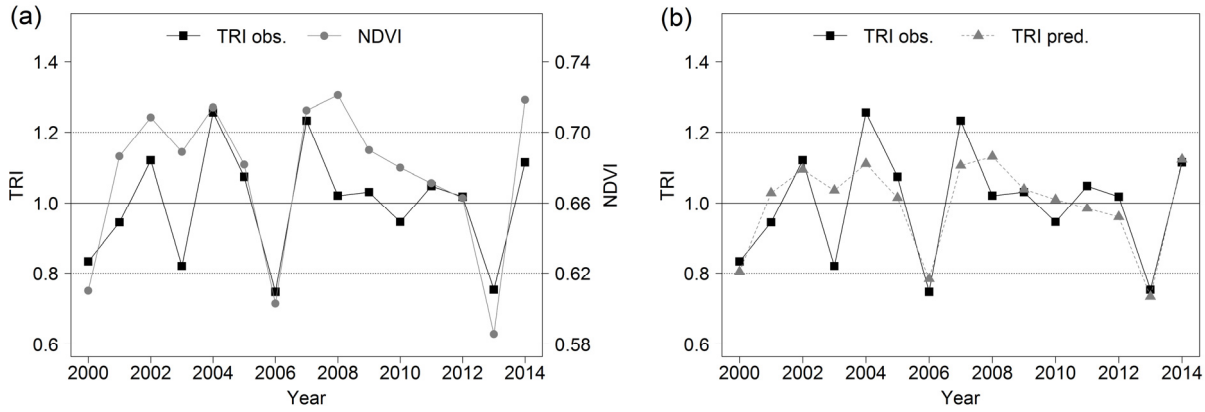

Figure 7: NDVI and TRI for dominant trees on plot 2 (a). NDVI represents the average of the four images from DOY 65 to 113 over all three pixel clusters. (b): Observed TRI 2000-2014 vs. values of the function described in the text and in Equation 2.

The NDVI in Fig. 7a was transformed to values between -1 and 1 according to Equation 1. On this basis the linear model for estimating TRI (TRI_m) for the selected data is represented by Equation 2:

$$TRI_m = -0.99071 + 2.9433 \times NDVI \qquad \text{Eq. 2}$$

The adjusted coefficient of determination of the model with the parameters described above is $R^2_{adj.} = 0.625$ with a bias of 0.01%, the Gleichlaeufigkeit between the time series of observed and predicted TRI is 0.8 or 80%, respectively. The precision of the model (Equation 2) according to Pretzsch (2001) is approximately 34%.

The correlation analyses indicated close relationships between TRI and NDVI for image series taken not only in spring but also in late summer. Fig. 6a shows high correlation coefficients for series whose first image was dated DOY 225, i.e. August 13. Testing all possible lengths of series similar to Fig. 6b we found maximum r values for NDVI derived as averages of the two images of DOY 225 and 241. These averages ($NDVI_{225\text{-}41}$) were then entered (i) as the only independent variables of a linear model and (ii) in combination with the average of four images starting on DOY 65 ($NDVI_{65\text{-}113}$). The results are given in Fig. 8, the respective equations are listed below.

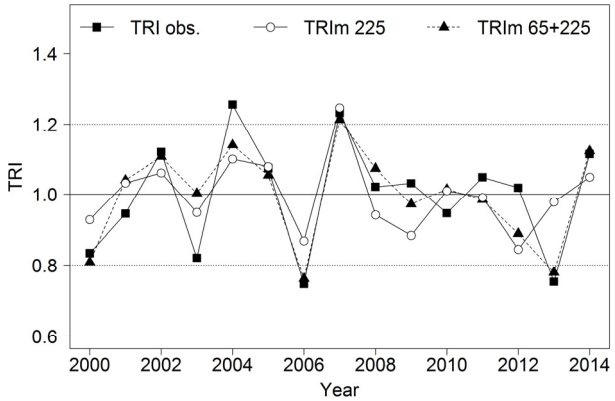

Fig. 8: TRI for dominant trees on plot 2 in the years 2000-2014 as observed (TRI obs.) vs. values of a simple linear function of NDVI over DOY 225+241 (TRIm 225) and values of a function using both NDVI 225-241 and NDVI 65-113 (TRIm 65+225); see also Equations 2, 3 and 4

$$TRI_{m\ 225} = -3.526 + 5.710 \times NDVI_{225\text{-}241} \qquad R^2_{adj.} = 0.391 \qquad \text{Eq. 3}$$

$$TRI_{m\ 65+225} = -2.9270 + 2.3228 \times NDVI_{65\text{-}113} + 2.9733 \times NDVI_{225\text{-}241} \qquad R^2_{adj.} = 0.697 \qquad \text{Eq. 4}$$

Discussion

Remote-sensing derived NDVI information is widely used to detect changes in the activity and thus in the density or vitality of vegetation (D'Arrigo et al. 2000, Kaufmann et al. 2008, Didan et al. 2015, Bhuyan et al. 2017). Several studies have investigated the relationships of NDVI data with annually variable indicators of productivity, either at the level of TRW or of wood density. Wang et al. (2004) and Bunn et al. (2013) have found significant correlations between tree-ring width and NDVI in forests in the American Middle West and in Siberia, respectively. Bunn et al. (2013) applied principal component analysis to test mean and accumulated NDVI data for their influence on TRW, TRI, and maximum latewood density (MXD). The latter was also employed by D'Arrigo et al. (2000) in their analyses of tree rings from boreal forests in Alaska and Siberia. This study also highlighted the close relationships between MXD variability and changes in productivity on an annual basis. The authors attributed the strength of this connection to the dependence on favourable temperatures in the vegetation period that is characteristic for both parameters.

In the regional context of Europe the capacity of MODIS NDVI data to reflect inter-annual variability in forest biomass activity was explored by, for example, Maselli et al. (2014). They have shown that NDVI information can be used to reliably estimate forest gross primary production in the exemplary Italian region of Tuscany. In contrast to that, Coulthard et al. (2017) found that NDVI in drought-stressed forests in Cyprus was coupled strongly to TRW only under certain ecological conditions while other conditions decoupled this relation, with shrub and grass productivity replacing tree growth as the primary representative of NDVI variability. In a study covering northeast Germany and western Poland (Schröder et al. 2014) the opportunities to predict forest net primary production based on remote sensing data were explored for the main forest types in the region. The achieved results were promising and led to the additional and more detailed investigations described here.

The forest stands selected to test our modeling approach represent typical conditions in the north-eastern part of Germany and cover the most important age span for the regionally dominant species *Pinus sylvestris*. Borer cores were extracted and data were processed according to standardized methods (Speer 2010). However, there were minor problems related to the sample size. In accordance with Bunn et al. (2013) we chose ten trees per sub-sample to be a sufficient sample size, but this number was in some cases reduced because we excluded samples deviating from the mean growth course of the respective sample following an approach promoted by Beck (unpublished, see Schröder 2015). While the Expressed Population Signal (EPS; Wigley 1984) was larger than 0.9 on all plots (with sample size = 20), the parameter was lower than 0.8 for the suppressed-trees sub-samples. An EPS > 0.85 is a reliable indicator for a sufficient similarity in the reaction to climate between the sample and the population it was taken from (Briffa and Jones 1990). The low EPS values in the suppressed-trees sub-samples resulted (i) from the reduction of sample size (one tree for plots 1 and 3 and two trees for plot 2) and (ii) from the larger disturbances due to competition that influence the climatic signal in trees with secondary social position (Speer 2010). Because the TRI time series derived for the sub-samples on all plots so closely resembled each other (see Fig. 3c) we decided to take them as representative for the respective stands and social groups. The important questions related to probably biased derivations of long-term growth trends as described by Nehrbass-Ahles et al. (2014) were irrelevant in our context because of the extreme brevity of the time series we used.

The robustness of the correlations could not only be observed with respect to the sub-samples selected as TRI data base (Fig. 5a) but also in relation to the source of the involved NDVI time series. While the highest coefficients result from correlations of TRI with "local", i.e. site-specific, NDVI series, the series of the average of all 3×9 pixels also yields reliable and statistically significant estimates of TRI with coefficients between r = 0.65 and r = 0.70 (for intervals between 10 and 14 years). Although the quality of representation is somewhat poorer than that of the plot-calibrated models, the linear equation for TRI on plot 2 presented in Fig. 7b and Eq. 2 can also

estimate TRI on plots 1 and 3 (Fig. 9). Years with particularly high or low TRI values are depicted rather well, and Gleichlaeufigkeit between the plot 2 TRI model and site-specific TRI is 80% on plot 1 (Fig. 9a) and plot 3 (Fig. 9b).

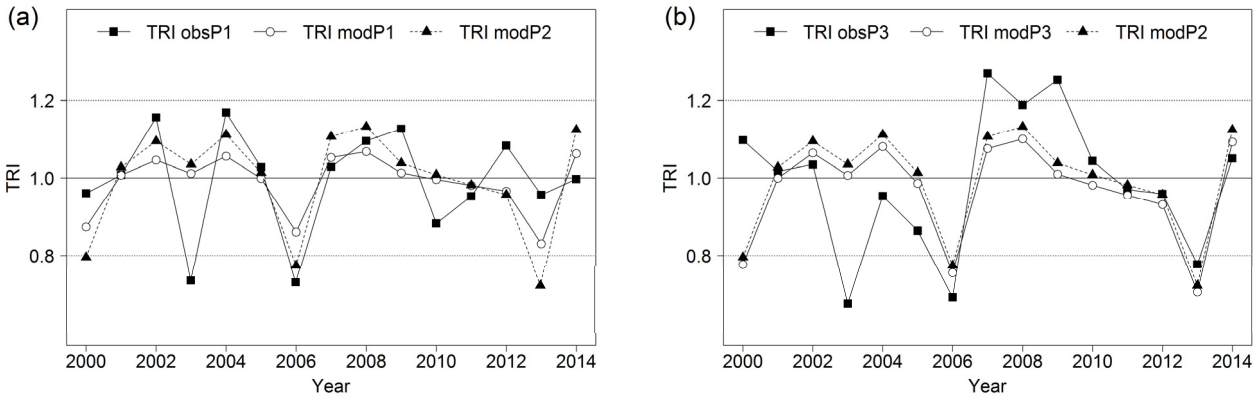

Figure 9: Representation of observed TRI (TRI obs) on plot 1 (P1) and plot 3 (P3) by simple linear models of average NDVI (TRI mod) calibrated either for the specific plot or for plot 2 (P2)

The investigated relations between remote sensing data and inter-annual productivity variation show a surprisingly high level of parallelism, most of all in their representation of the deviation from average conditions. However, the derived models should not be extrapolated without any prior studies for other tree species, structural compositions of stands, site types, or time intervals differing from the objects of our study. The relatively short period of availability for the Terra/MODIS data (2000-2014) limited the temporal calibration window accessible for modeling. Alternative sources such as the NOAA-AVHRR data series which are based on identical formulae (Tucker 1979) could extend the information available for calibration back to 1981 (D'Arrigo et al. 2000; Didan et al. 2015). However, the wider spatial grid (i.e. the more coarse resolution) of the older data set which is 1.09×1.09 km has also to be acknowledged.

The NDVI information in the applied data set is derived from the "best" images within a 16-day interval with the smallest possible influence of meteorological and atmospheric disturbances. In the MOD13Q1 product the individual values are characterized by a parameter that expresses the quality of this "best possible" image (Didan et al. 2015). While in this study all available NDVI data were used for calibration, further research could focus on input data of only the highest quality level. Pre-whitening methods such as smoothing splines and Savitzky-Golay filters should be tested for their capacities to improve coherence and plausibility in the NDVI time series. The Enhanced Vegetation Index (EVI) integrating more wavelengths than Tucker's (1979) NDVI is capable of productivity estimations for structurally diverse, multi-layered forests (Huete et al. 2002). Future studies might compare the opportunities of modeling TRI from EVI to the results presented here. New ways should also be tested to represent biomass productivity in the respective models: Apart from TRI, tree growth and biomass production can also be derived from basal area, volume, or dry matter increment (Pretzsch 2009). To obtain reliable estimates for these parameters, however, additional data are necessary that were not available for our study.

Conclusion

Our results show that statistical growth simulations may benefit substantially from the integration of remote sensing data particularly when growth data with annual resolution are not available and at the same time annually resolved estimations are expected. As a crucial element to evaluate the relations between tree growth and satellite data, tree-ring width and tree-ring index (TRI) time

series have proved to be of especially valuable. However, to follow the methodological way presented here, precise and reliable input data are required both on the remote sensing and on the "ground-truthing" side, and the dependency of possible results on the specific site and temporal conditions should always be recognized. We have proven very close correlations between NDVI and TRI time series that were robust throughout various age classes for homogenous, even-aged conifer stands, but the existence of similar relations in multi-species, uneven-aged stands has still to be confirmed.

References

Bhuyan, U., Zang, C., Vicente-Serrano, S. M., Menzel, A. (2017): Exploring Relationships among Tree-Ring Growth, Climate Variability, and Seasonal Leaf Activity on Varying Timescales and Spatial Resolutions. Remote Sensing 9 (526) 13 pp., doi:10.3390/rs9060526

Brewer, P., Murphy, D., Jansma, E. (2011): TRiCYCLE: a universal conversion tool for digital tree-ring data. Tree-Ring Research 67 (2): 135–144

Briffa, K. R., Jones, P. D. (1990): Basic chronology assessment and statistics. In: Cook, E. R., Kairiukstis, L. A. (eds.): Methods of Dendrochronology. Applications in the Environmental Sciences. Kluwer Academic Publ., Dordrecht: 137-152

Bunn, A. (2008): A dendrochronology program library in R (dplR). Dendrochronologia 26: 115-124

Bunn, A., Hughes, M. K., Kirdyanow, A. V., Losleben, M., Shishov, V. V., Berner, L. T., Olchev, A., Vaganov, E. A. (2013): Comparing forest measurements from tree rings and a space-based index of vegetation activity in Siberia. Environmental Research Letters 8 (3): 035034 (8 S.)

Bunn, A., Korpela, M., Biondi, F., Campelo, F., Mérian, P., Qeadan, F., Zang, C. (2015): dplR: Dendrochronology Program Library in R. R package version 1.6.2. https://cran.r-project.org/package=dplR

Coulthard, B. L., Touchan, R., Anchukaitis, K. J., Meko, D. M., Sivrikaya, F. (2017): Tree growth and vegetation activity at the ecosystem-scale in the eastern Mediterranean. Environmental Research Letters 12, 084008, 10 pp., https://doi.org/10.1088/1748-9326/aa7b26

D'Arrigo, R. D., Malmstrom, C. M., Jacoby, G. C., Los, S. O., Bunker, D. E. (2000): Correlation between maximum latewood density of annual tree rings and NDVI based estimates of forest productivity. International Journal of Remote Sensing 21 (11): 2329–2336

Didan, K., Barreto Munoz, A., Solano, R., Huete, A. (2015): MODIS Vegetation Index User's Guide (MOD13 Series). Vegetation Index and Phenology Lab. The University of Arizona. Available at: http://vip.arizona.edu/documents/MODIS/MODIS_VI_UsersGuide_June_2015_C6.pdf (07.06.2016)

Hijmans, R. J. (2015): raster: Geographic Data Analysis and Modeling. R package version 2.5-2. https://cran.R-project.org/package=raster

Huete, A., Didan, K., Miura, T., Rodriguez, E. P., Gao, X., Ferreira, L. G. (2002): Overview of the radiometric and biophysical performance of the MODIS vegetation indices. Remote Sensing of Environment 83 (1): 195–213

Kaufmann, R. K., D'Arrigo, R. D., Paletta, L. F., Tian, H. Q., Matt Jolly, W., Myneni, R. B. (2008): Identifying Climatic Controls on Ring Width: The Timing of Correlations between Tree Rings and NDVI. Earth Interactions 12 (14), 14 pp., doi: 10.1175/2008EI263.1

Maselli, M., Cherubini, P., Chiesi, M., Gilabert, M. A., Lombardi, F., Moreno, A., Teobaldelli, M., Tognetti, R. (2014): Start of the dry season as a main determinant of inter-annual Mediterranean forest production variations. Agricultural and Forest Meteorology 194: 197–206

Nagel, J., Duda, H., Hansen, J. (2006): Forest Simulator BWINPro7. Forst und Holz 61 (10): 427-429

NASA (2016): Measuring vegetation NDVI & EVI. Normalized Difference Vegetation Index (NDVI). http://earthobservatory.nasa.gov/Features/MeasuringVegetation/measuring_vegetation_2.php (27.05.2016)

NASA (2016a): Vegetation Indices 16-Day L3 Global 250m. https://lpdaac.usgs.gov/dataset_discovery/modis/modis_products_table/mod13q1 (01.06.2016)

Nehrbass-Ahles, C., Babst, F., Kleese, F., Nötzli, M., Bouriaud, O., Neukom, R., Dobbertin, M., Frank, D. (2014): The influence of sampling design on tree-ring based quantification of forest growth. Global Change Biology 20 (9): 2867-2885

Pebesma, E. J., Bivand, R. S. (2005): Classes and methods for spatial data in R. R News 5 (2), http://cran.r-project.org/doc/Rnews/ (02.06.2016)

Pretzsch, H. (2001): Modellierung des Waldwachstums. Paul Parey, Hamburg, Berlin

Pretzsch, H. (2009): Forest dynamics, growth and yield: From measurement to model. Springer Verlag, Berlin.

R Core Team (2015): R: A language and environment for statistical computing. R Foundation for Statistical Computing, Vienna, Austria

Schröder, J., Lehmann, P., Lessing, R., Körner, M. (2014): Zuwachsschätzung per Satellit? Potenziale fernerkundungsbasierter Biomassemodelle am Beispiel der Euroregion "POMERANIA". In: Kohnle, U., Klädtke, J. (Hrsg.): Sektion Ertragskunde im DVFFA, Beiträge zur Jahrestagung in Lenzen 2014: 46-56

Schröder, J. (2015): Zum Einfluss der Witterung auf Wuchsverhalten und Vitalität der Trauben-Eiche (*Quercus petraea* [Matt.] Liebl.). Eugen Ulmer, Stuttgart, Dresden

Speer, J. H. (2010): Fundamentals of Tree Ring Research. Tucson: University of Arizona Press

Stabler, B. (2013): shapefiles: Read and Write ESRI Shapefiles. R package version 0.7. https://cran.r-project.org/package=shapefiles

Tucker, C. J. (1979): Red and photographic infrared linear combinations for monitoring vegetation. Remote Sensing of Environment 8 (2): 127-150

Wang, J., Rich, P. M., Price, K. P., Kettle, W. D. (2004): Relations between NDVI and tree productivity in the central Great Plains. International Journal of Remote Sensing 25 (16): 3127–3138

Pointer years in beech in the region of Žagubica, Eastern Serbia

B. Stajić[1], M. Kazimirović[1], Z. Baković[2] & V. Dukić[3]

[1] University of Belgrade, Faculty of Forestry, Belgrade, Serbia
[2] Public Enterprise ''Srbijašume'', Belgrade Serbia
[3] University of Banja Luka, Faculty of Forestry, Banja Luka, Bosnia and Herzegovina
E-mail: branko.stajic@sfb.bg.ac.rs

Introduction

The beech (*Fagus* silvatycai) is in Serbia naturally distributed in a wide range of different climate and site conditions and on optimal sites it can grow over 45 m in height and 1.5 m in diameter (Vučković & Stajić 2005). A culmination of diameter and height increment in good site conditions generally occurs between 20 and 30 years of age (Stajić 2010). Since it grows in a wide horizontal and vertical variation of ecological conditions, and since it is well synchronised with other tree species and highly sensitive to climate, beech is a useful tree species to highlight the effects of environmental changes related to climate (Piovesan et al. 2003, Di Filippo el al. 2013, Roibu et al. 2017).

As long-living organisms, trees provide a record of past growing conditions in their annual rings (Scharnweber et al. 2011). Therefore, the widths of annual growth rings (radial increment values) reflect the nature of physiological processes (Lebourgeois et al. 2005), and their chronologies can be considered as natural archives of the interaction between trees and their surroundings (Stajić et al. 2015).

Abrupt changes in the environment lead to the formation of particularly narrow or wide tree rings which are called 'event years' at the individual tree level, whereas the term 'pointer year' refers to specific rings with remarkable widths at the stand level (Schweingruber et al. 1990). Proper attribution of these exceptionally narrow or wide increments to the corresponding calendar years, and their use in chronology synchronization is the essence of the fundamental dendrochronological procedure of cross-dating (Douglass 1939). Furthermore, the occurrence of pointer years has a special significance in dendroclimatological research studies because they are most often caused by extreme climate events. Investigations of this kind of a relationship entail a search for statistical dependences mostly between pointer years and monthly temperatures and precipitation (Fritts 1976, Schweingruber et al. 1990).

The available literature on pointer year determination offers two distinct methodological approaches. The first method was originally introduced by Cropper (1979) and implies using normalization in a symmetrically moving window, while Schweingruber et al. (1990) proposed an approach based on the relative growth change ratio. Besides them, there are several other procedures which essentially represent modifications of these two approaches (Becker et al. 1994, Lebourgeois et al. 2005, Neuwirth et al. 2007).

The primary objectives of this paper were 1) to detect pointer years by applying several methodological procedures, 2) to analyse the number and the character of the obtained sets of pointer years and to emphasize the years which were recognized by more than one method, as well as 3) to study a relationship between the obtained pointer years and climate variables.

Data

The primary research material was compiled from 32 trees (64 cores).The sample was collected in a beech stand located on the territory of Žagubica municipality in Eastern Serbia in autumn 2013 (Fig. 1).This is an even-aged and lightly thinned pure stand of high origin, located in the altitude range from 890 to 1030 m above sea level, with the centre of the area at 21° 43.5' longitude and 44° 6.5' latitude.

The prevailing climate can be characterized as continental with quite cold and humid winters, and mild and fresh summers. The nearest meteorological station is located at a significantly lower

elevation and its position has been changed several times in the past, which makes its data records unrepresentative. Therefore, the mean monthly temperature and the sum of precipitation were obtained from KNMI Climate explorer by using CRU TS3.24.01 land dataset at 0.5° spatial resolution. The longest available set of row data was taken over for a single grid point nearest to the centre of the research area.

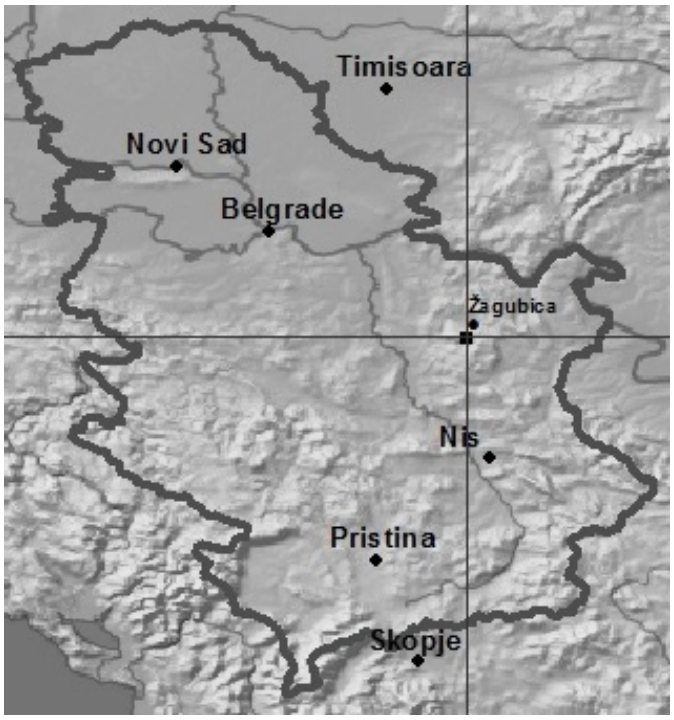

Figure 1: The location of the studied area.

Methods

The selected tree-ring series were subjected to a strict cross-dating procedure. For this purpose, they were divided into the segments of a 40-year length and a 20-year overlap. This primary network was moved across the chronologies by one-year step in order to cover all parts equally. All the series whose overall correlation with the master chronology was below 0.5 were removed from the selection, as well as the series with one or more insignificantly correlated segments.

Determination of the event years for the longest common period was conducted using eight different procedures. The approach presented by Schweingruber et al. (1990) relates tree growth in a particular year to the average growth of four preceding years. According to them, "…*an event year occurs when the ring width is at least by 40% smaller or by 60% wider than the average of the preceding four years*…". However, Becker et al. (1994) modified this method by adopting a different threshold, assuming that event years have 10% growth change compared to the previous one. Cropper's approach (1972) was further used. It implies the utilization of mean and standard deviations as indicators of relative narrowness. The calculation of these so-called Cropper values (C values) was carried out by applying a moving window composed of 5, 7 and 13 consecutive tree rings. Additionally, identification of event year with this method was conducted by using two types of thresholds. According to Cropper (1972), an event year should exceed 0.75 of the window standard deviation, while Neuwirth et al. (2007) differentiate weak (C values > 1), strong (C values > 1.28) and extreme (C values > 1.645) event years. Thereafter, the identification of pointer years was accomplished by using the statistical criterion suggested by Eckstein & Bauch (1969). In order to examine the connection between pointer years and the trends in climate data, we used a similar approach of correlation analysis proposed by Lebourgeois et al. (2004). All the necessary calculations were done in the R environment (R core team 2008) by using PointRes (Van der Maaten-Theunissen et al. 2015) and dplR (Bunn et al. 2008) packages and some personal codes.

Results

The rigorous synchronization procedure reduced the total sample to 26 highly correlated tree chronologies (average interserial correlation r_{xy}=0.71). The remaining series were then truncated to the common period which covers a time sequence between 1932 and 2013. Eight different procedures determined a total of 27 pointer years (32.5%) in this period. Extremely narrow tree rings occurred in 16 years, while remarkably wide rings were detected 11 times (Fig. 2). In total, the Becker's procedure ascertained the largest number of pointer years (23), the majority of which (19) were unique to this method. However, the procedure based on 5-year long normalization window in combination with the thresholds proposed by Neuwirth failed to recognize any year as exceptional.

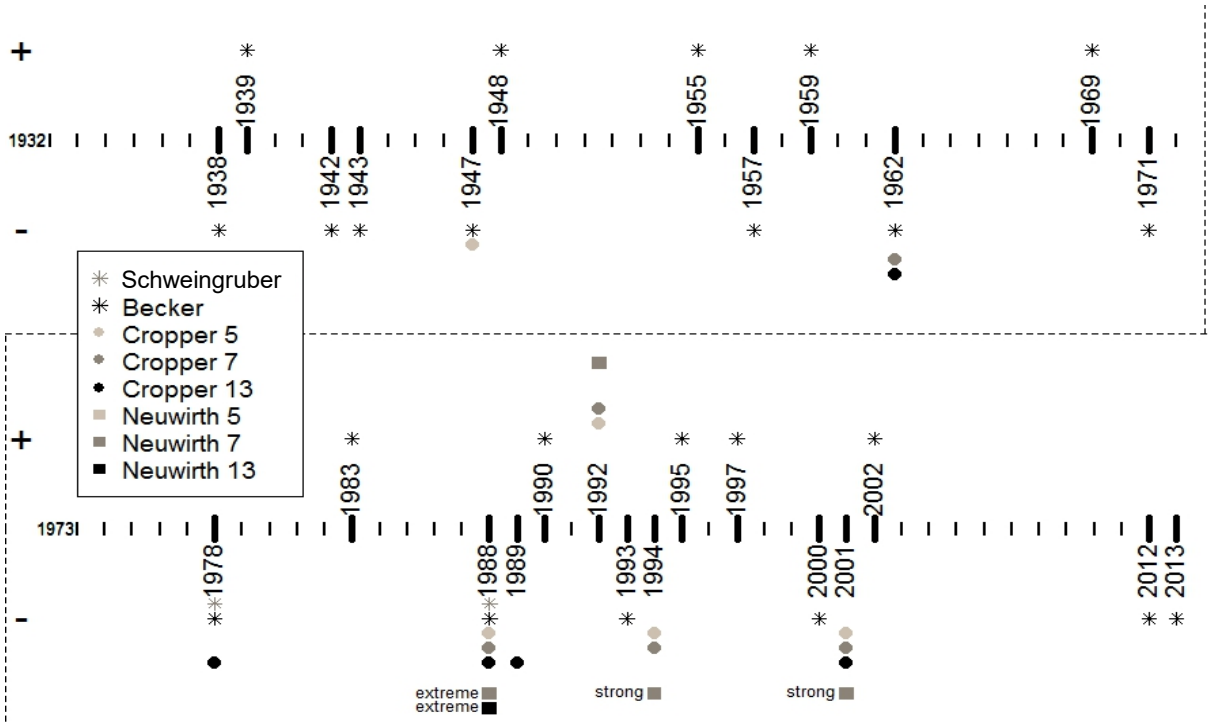

Figure 2: The pointer years determined by 8 various methodological procedures for period 1932-2013.

Seven pointer years were detected by more than one procedure, six of which were negative and only one positive. The tree ring formed in 1988 was recognized as conspicuously narrow by almost all procedures (7/8). Some procedures stressed negative trends of radial increment in the following years: 2001 (4/8), 1962, 1978, 1994 (3/8) and 1947 (2/8). The only positive remarkable growth response detected by several procedures (3/8) occurred in 1992.

In order to evaluate the impact of simple climatic parameters on the occurrence of pointer years, monthly precipitation and temperature data were correlated with the amounts of Mean relative growth change (MRGC in %) and Mean Cropper values (MCV in mm). All the obtained pointer years, divided into two subsets, show significantly positive correlations with June precipitation (JP in mm/m^2) (Fig. 3). Additional research discovered that pointer years have a less significant correlation (p<0.10) with March precipitation (not shown), while the relationship with the previous August rainfall was visible but insignificant. However, the mean monthly temperature did not show any relationship with the pointer years. The analysis of June precipitation showed that more than a half of the pointer years follow above and below average trends (15 out of 27 or 56%) and the majority of them lay on prominent tops. The rest of the identified exceptional increments could be associated in the same way with the current March and the previous August precipitation. However, those 7 and 5 pointer years coincided with less expressed peaks (Fig. 4).

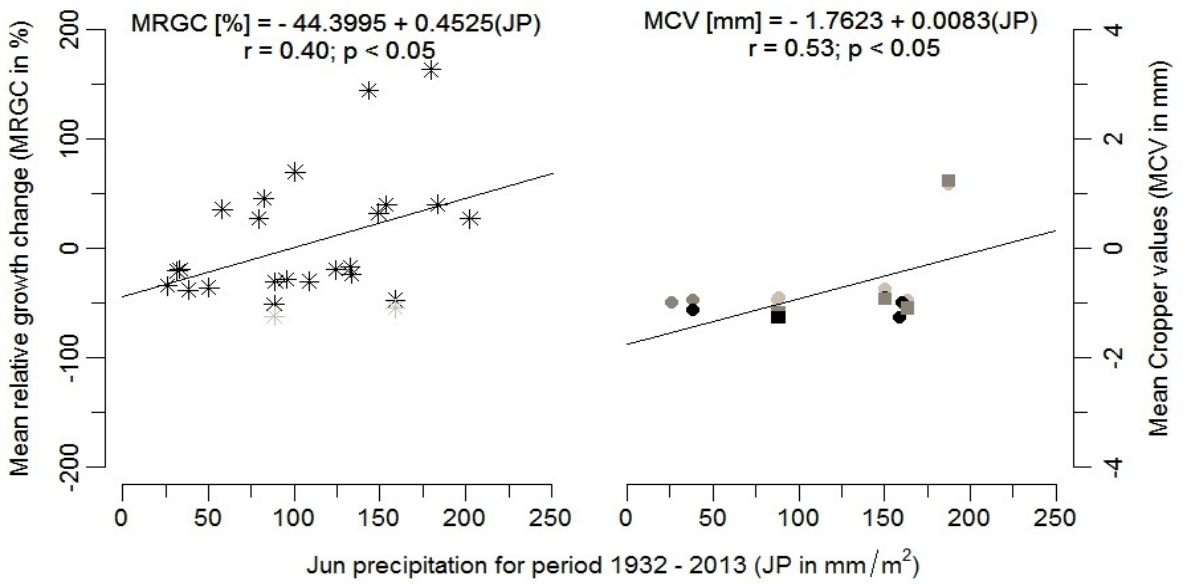

Figure 3: The correlation between pointer year's Mean Relative Growth Change (MRGC in %) and Mean Cropper Values (MCV in mm) with the sums of June precipitation (JP in mm/m^2) for the period between 1932 and 2013.

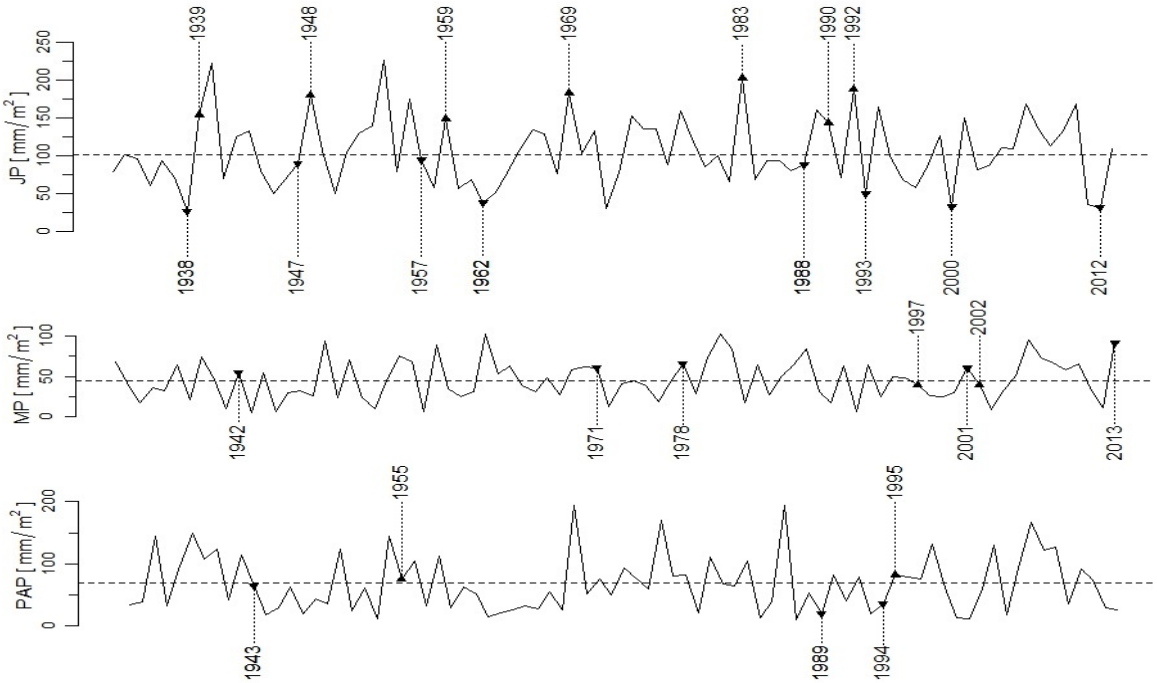

Figure 4: The relationship between the above or below average precipitation trends in June, March and previous August (JP, MP, and PAP in mm/m^2) and the occurrence of pointer years. The dotted lines presents the average monthly precipitation for the period between 1932 and 2013.

Discussion and conclusion

The analysis of pointer years provides additional information about the radial growth response of trees to the abrupt changes in their surroundings. However, when it comes to the determination of pointer years, it is often hard to choose which of the presented methodological approaches or procedures should be applied. The selection is further hindered by the fact that Cropper (1972) and Schweingruber et al. (1990) have missed providing ultimate instructions for the following: 1) how to select the proper number of neighbouring tree rings for the comparison with the increments in the observed year and 2) how to adopt the appropriate threshold for the identification of negative or

positive growth changes at the tree level. Such situation has left room for subjective interpretations of these criteria, which resulted in the number of various modified procedures (Becker et al. 1994, Lebourgeois et al. 2005, Neuwirth et al. 2007). This issue has already been pointed out by Sz. Bijak (2007), who demonstrated how different combinations regarding the mentioned criteria affect the number of identified pointer years. The author also concluded that in order to obtain comparable results "…*different aspect of the determination process seems to require more detailed specification*...". In that sense, Neuwirth et al. (2007) tried to standardize the event year threshold by using a probability density function of the standardized normal distribution. Therefore, it is still questionable whether the adopted threshold values (10%, 20% and 33%) could be different.

The obvious lack of precise criteria for the determination of exceptional increments at the tree level can be overcome in the case of pointer years by applying the thresholds which are statistically related to the number of trees in the sample (Ecstein & Bauch 1969). Nevertheless, the application of different event year thresholds affect the results in terms of the total number and the nature of pointer years and it is still unclear how to decide which one to use for most reliable outcomes. One of the possible solutions could be the simultaneous use of several procedures in order to determine the pattern of the pointer years detected by more than one routine.

In the light of the aforementioned, seven pointer years have fulfilled the adopted requirements. Nevertheless, most often it is really hard to compare the obtained results even with those from nearby regions because different researchers apply different procedures (Mayer 1998/199). However, the negative 1947, 1962, 1988 and 2001 are in accordance with the results presented by Stajić (2014) for the beech in the nearby area of the "Djerdap" National Park. This research study determined pointer years by applying only the method after Schweingruber (1983) and that could be one of the reasons why the results are not in full agreement. Furthermore, two of the identified negative pointer years correspond to the results of Neuwirth et al. (2007) who conducted comprehensive spatial analyses of pointer year occurrence for the Central Europe and concluded that the climatological situation during 1947 and 1962 caused negative growth response on lower mountain sites.

The investigation of climatic forcing of the single pointer years clearly showed that the amount of June precipitation is associated with the occurrence of 56% of the observed extreme years. Such results are in accordance with the previous findings which stressed the importance of summer precipitation for beech growth response all across Europe (Piovesan et al. 2005; Lebourgeois el al 2005; Meirandus et al. 2012). The March precipitation seemed to play a particularly important role in the formation of seven exceptional increments, probably because the amount of precipitation in this part of the year can affect the soil structure in such a way that the excess water can postpone the growing season (Becker et al. 1994). Furthermore, the last four unexplained pointer years coincide with the precipitation trends from August of the previous growing season. This kind of relationship has already been reported for beech trees in similar altitudinal ranges (Neuwirth et al. 2007; Di Filippo et al. 2007). Unlike precipitation, the obtained results suggest that temperature anomalies do not have a direct influence on the pointer year determination.

It can be concluded that the pointer years determined by more than one procedure are in accordance with those observed in the previous studies in nearby areas as well as in distant parts of Central Europe. Therefore, it could be useful to use multiple procedures simultaneously in order to evaluate the potential of this approach for establishing the network of pointer years of a wider area. The significant influence of the climate on the occurrence of pointer years was detected, but none of the analysed parameters could be solely responsible for exceptional growth responses. Although the impact of the conducted light thinning on the determined climate-growth relationship of here studied dominant beech trees is probably rather poorly expressed, it could be useful to check the obtained results by the use of linear mixed modelling for tree-ring standardization. Having to face this problem and the need for more representative information on beech climate-growth relationship, the obtained results call for a more complex growth-climate analysis, including a deeper data standardization procedure, the application of additional climate-growth data, dendroclimatic methods and parameters.

Acknowledgements

This paper was realized as a part of the project "Studying climate change and its influence on the environment: impacts, adaptation and mitigation" (43007) financed by the Ministry of Education and Science of the Republic of Serbia within the framework of integrated and interdisciplinary research for the period 2011-2016.

References

Becker, M., Nieminen, T., Geremia, F. (1994): Short-term variations and long-term changes in oak productivity in northeastern France. The role of climate and atmospheric CO_2. *Annales des sciences forestieres*, INRA/EDP Sciences, 51 (5): 477-492.

Bijak, Sz. (2008): Various factors influencing the pointer year analysis. In: Elferts, D. et al.: TRACE 6- Proceedings of the DENDROSYMPOSIUM 2007, May 3rd – 6th 2007, Riga, Latvia: 77-82.

Bunn, A.G. (2008). A dendrochronology program library in R (dplR). *Dendrochronologia,* 26(2): 115–124.

Cropper, J. P. (1979): Tree-ring skeleton plotting by computer. *Tree-ring Bulletin* 39: 47-59.

Di Filippo, A., Biondi, F., Ziaco, E., Piovesan, G. (2013): Dendroecological networks to investigate forest dynamics: The case of European beech in Italy. In: Helle, G et al.: TRACE 10- Proceedings of the DENDROSYMPOSIUM 2012: May 8th - 12th, 2012 in Potsdam and Eberswalde, Germany: 134-143.

Douglass, A. E. (1939): Crossdating in dendrochronology. *Journal of Forestry* 39: 825-831.

Eckstein, D., Bauch, J. (1969): Beitrag zur Rationalisierung eines dendrochronologischen Verfahrens und zur Analyse seiner Aussagesicherheit. *Forstwissenschaftliches Centralblatt* 88 (1): 230–250.

Fritts, H. C. (1976): Tree rings and climate. Academic Press, London.

Lebourgeois, F., Breda, N., Ulrich, E., Granier, A. (2005): Climate-tree-growth relationships of European beech (*Fagus sylvatica* L.) in the French Permanent Plot Network (RENECOFOR). *Trees* 19: 385–401.

Meinardus, C., Bayer, E. M., Lasermann, B., Singer, A., Bräuning, A. (2012): Reactions and recovery times of Fagus sylvatica after drought events derived from of ring width and maximum latewood density. In: Gärtner, H. et al.: TRACE 10- Proceedings of the DENDROSYMPOSIUM 2012: May 8th - 12th, 2012 in Potsdam and Eberswalde, Germany: 93 - 98.

Meyer, F. D. (1998/1999): Pointer years analysis in dendroecology: a comparison of methods. *Dendrochronologia* 16-17: 193-204.

Neuwirth, B., Schweingruber, F.H., Winiger, M. (2007): Spatial patterns of Central European pointer years. *Dendrochronologia* 24: 79-89.

Piovesan, G., Bernabei, M., Di Filippo, A., Romagnoli, M., Schirone, B. (2003): A long-term tree ring beech chronology from a high-elevation old growth forest of Central Italy. *Dendrochronologia*, 21: 13–22.

Piovesan, G., Biondi, F., Bernabei, M., Di Filippo, A., Schirone, B. (2005): Spatial and altitudinal bioclimatic zones of the Italian peninsula identified from a beech (*Fagus sylvatica* L.) tree-ring network. *Acta Oecologica* 27:197-210.

R Development Core Team (2008) R: a language and environment for statistical computing. R Foundation for Statistical Computing, Vienna, Austria. http://cran.r-project.org/

Roibu, C. C., Popa, I., Kirchhefer, A J., Palaghianu, C. (2017): Growth responses to climate in a tree-ring network of European beech (*Fagus sylvatica* L.) from the eastern limit of its natural distribution area. *Dendrochronologia* 42: 104–116

Scharnweber, T., Manthey, M., Criegee, C., Bauwe, A., Schroder,C., Wilmking, M. (2011): Drought matters – Declining precipitation influences growth of *Fagus sylvatica* L. and *Quercus robur* L. in north-eastern Germany. *Forest Ecology and Management* 262: 947-961.

Schweingruber, F. H. (1983): Der Jahring. Verlag Paul Haupt Bern und Stuttgart.

Schweingruber, F. H., Eckstein, D., Serre-Bachet, F., Bräker O. U. (1990): Identification, presentation and interpretation of event years and pointer years in dendrochronology. *Dendrochronologia 8*: 9-38.

Stajić, B. (2010): Characteristics of the stand structure and the tree growth in the mixed stands of beech and valuable broadleaved tree species in the National park "Djerdap". The University of Belgrade, the Faculty of Forestry, 331 p., (in Serbian).

Stajić, B., Vučković, M., Janjatović, Ž. (2015): Preliminary dendroclimatological analysis of Sessile oak (*Quercus petraea* (Matt.) Liebl.) in “Fruška Gora” National park, Serbia. *Baltic forestry* 21 (1): 83-95.

Stajić, B. 2014. Pointer years in the growth of beech trees of the NP "Đerdap" area. *Bulletin of the Faculty of Forestry* 110: 175-188, (in Serbian)

Van der Maaten-Theunissen, M., Van der Maaten, E., Bouriaud, O. (2015). PointRes: An R package to analyse pointer years and components of resilience. *Dendrochronologia, 35*: 34-38.

Vučković M., Stajić B. (2005): Growth and productivity of beech. In: Stojanović, Lj., (ed.) Beech in Serbia. The Society of the forest engineers and the technicians of Serbia, The University of Belgrade, the Faculty of Forestry, Belgrade, 352-364, (in Serbian)

Quantifying the influence of westerly wave trains on moisture variations on the southeastern Tibetan Plateau using tree-ring stable oxygen isotopes

Jakob Wernicke[1] , Haifeng Zhu[2], Achim Bräuning[1]

[1]Friedrich-Alexander University Erlangen-Nuremberg (Germany)
[2]Institute of Tibetan Plateau Research, Chinese Academy of Sciences, Beijing (China)
Email: jakob.wernicke@fau.de

Introduction

Increasing global mean air temperatures are supposed to induce a strengthening of the Asian Summer Monsoon moisture supply over large parts of Asia (Ma and Yu, 2014). However, the spatial heterogeneity of monsoonal rain requires region-specific considerations (Conroy & Overpeck 2011, Wernicke et al. 2015). For instance, tree-ring $\delta^{18}O$ based hydroclimatic reconstructions from the southeastern Tibetan plateau (TP) revealed a distinct drying trend since the ~1850s (Liu et al. 2013, Shi et al. 2012, Wernicke et al. 2017). Wernicke et al. 2017 attributed this trend to a frequency increase of westerly wavetrains, which are supposed to impede the meridional moisture transport from the Bay of Bengal. The present study aims to quantify the impact of wave trains on moisture variations at the southeastern TP.

An increasing number of publications discuss the role of westerlies for controlling the north hemispheric moisture variability (Bothe et al. 2011, Ding and Wang 2005, Joseph and Srinivasan 1999, Saeed et al. 2011). It has been shown that the westerlies link the hydroclimate of Europe, Western Asia and the southeastern TP (Bothe et al. 2009, Mölg et al. 2014). The process is described as a transport of stationary wave energy from western Europe high latitudes, further downstream to western central Asia (Zhu et al. 2011). Centers of Rossby wave train action are clearly visible in one-point spatial correlation results computed for ERA20C humidity data (Wernicke et al. 2017). Generally, Rossby waves play a crucial role for the development of baroclinic instability that results in surface-cyclogenesis (Glatt & Wirth 2014). Therefore, Glatt & Wirth 2014 introduced an automatic algorithm for the detection of upper-tropospheric Rossby wave trains (RWT).

Here, we use their algorithm to investigate our hypothesis that RWT induced severe weather at the southeastern TP, where we collected moisture sensitive tree-ring samples and build a reliable d18O chronology (Wernicke et al. 2017). We examined the north hemispheric 250hPa meridional wind field (ERA20C) during 1960-2010. Although an influence might be reasonable, our preliminary analyses showed no statistically reliable associations. For this reason, we focused our further analyses on the geopotential field variability, which is supposed to display the polar-front position and thus an influence of subtropical (polar) air in the study region.

Material and Methods

We use the youngest part of a 660 years long $\delta^{18}O$ chronology from *Picea balfouriana*, growing on the southeastern TP (MiMei: 29°27'N, 96°26'E, ~3950m asl, see Figure 1). During the calibration period (1960-2010), the chronology shows significant negative correlations to summer season precipitation amounts (June-August, for details see Wernicke et al. 2017). The summer season precipitation reconstruction widely coincides with nearby precipitation reconstructions and shows wetter conditions during the LIA and a drying trend since the termination of the LIA. Additionally, monthly precipitation data from climate station Bomi were examined in this study (29°52'N, 94°46'E, 2736 m asl, data source: Chinese Meteorological Administration). RWT's are visually

detectable in so-called Hovmöller diagrams, which display the zonal variation of the mean meridional wind component (v-wind). Accordingly, we utilized v-wind reanalysis data (250hPa) provided by the European Centre of Medium-Range Weather Forcasts (ERA20C, Poli et al. 2013). The data span 1960-2010 and cover the whole northern hemisphere with a spatial resolution of 0.5°. We selected the 250hPa v-wind field in order to achieve free atmospheric conditions that are not affected by the rugged topography of the TP (surface roughness). This is particularly important, since RWT's are formed in the upper troposphere and large parts of the TP are situated at the 550hPa level (~4000m absl). According to the summer season precipitation sensitivity of our chronology (June-August, Wernicke et al. 2017), all analyses were tailored to these three summer months.

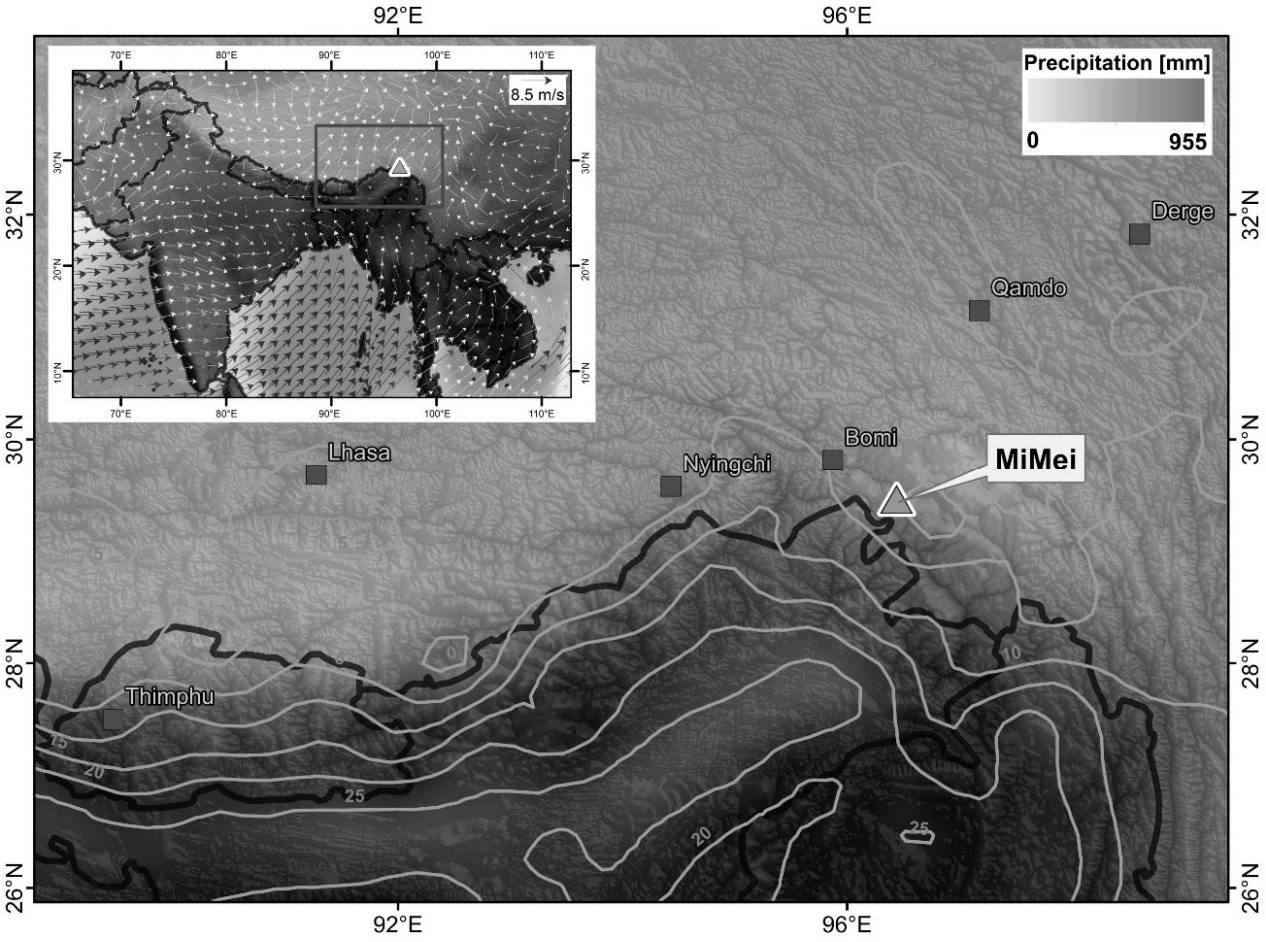

Figure 1: MiMei tree-ring $\delta^{18}O$ chronology location adapted from Wernicke et al. 2017. Gray lines display 5°C isotherms of the 2 m surface temperatures and blue color encodes mean precipitation amounts during May to October (data: High Asia Refined analysis (HAR, 2001-2011) (Maussion et al. 2014)). Background topographical data were provided by the Land Processes Distributed Active Archive Center (LP DAAC) and ASTER GDEM (product of METI and NASA). Wind vectors of inlay map display May to October average 10 m wind derived from HAR data.

Mathematically, RWT's are described as $v(\lambda,t) = Re[E(\lambda,t)e^{ik\lambda}]$, with $e^{ik\lambda}$ as the carrier wave (λ = wave number) and $E(\lambda,t)$ as its envelope (waves' amplitudes, Glatt & Wirth 2014). To capture RWT's envelopes, Zimin et al. 2003 proposed the application of Hilbert transformations. The algorithm is composed of a (i) Fourier transformation of the real function, (ii) inverse Fourier transformation within the range of synoptically meaningful wave numbers, and (iii) the actual envelope computation by integrating (i) and (ii) (Zimin et al. 2003). However, the Hilbert transformation describes plane wave structures and does not account for non-linear processes,

typically characterizing atmospheric processes. Accordingly, we followed the proposed remedies of Wolf & Wirth (2015) to adequately cope with this issue. In this pilot study, we primarily focus on the envelope presence-absence frequency. For that purpose, we investigated the envelope presence/absence during the eight driest and wettest years recorded at climate station Bomi. The numbers of envelopes were summed within an area of 20°-40°N over the northern hemisphere (180°W-180°E) and our particular study area (92°-98°E). Lastly, geopotential data ($\phi[m^2s^{-2}]$) were utilized to potentially localize the polar front position (Poli et al. 2013). Depending on earth's gravity field, the geopotential is larger at higher latitudes (and vice versa).

Results and Discussion

As displayed in figure 2, the Hovmöller diagrams unravel envelope clusters in the Pacific ocean (~150°W), which propagate within ~20 days eastward up to ~50°E (e.g. (b), (d), (e), (k), (o) in Figure 2). Moreover, it appears that envelopes form more frequently during the early summer season (June) and progressively occur less often until August. Envelopes at our study site occurred in 22 years during the period 1968-2010. As exemplary illustrated in Figure 2, we selected the eight driest (wettest) years (mean summer season precipitation +/-1σ) recorded at climate station Bomi and tested for mean differences in envelope abundance between both groups. Over the entire north hemispheric subtropical latitudes (20°-40°N), 17287 envelopes were counted during the wettest and 14668 during the driest years. Within the study area, 46 envelopes occurred during the wettest and 41 during the driest years, respectively. However, the envelope abundance distribution violates the normal distribution assumption (qq-plot not shown). Accordingly, we applied non-parametric statistical analyses in the further analyses (Leyer & Wesche 2007). Mann-Whitney-U test results revealed a true Null-hypothesis (H_0: $\mu_1 = \mu_2$), implying no differences in the average amount of envelopes during wet and dry years, neither within the subtropics ($p = 0.65$), nor within our study area on the TP ($p = 0.78$). Spearman correlations during the eight driest years revealed significant negative associations of summer season precipitation amounts and envelope abundance over the entire northern Hemisphere between 20°-40°N/180°W-180°E ($\rho = -0.81$, $p < 0.05$). Unfortunately, a similar result was not confirmed in correlation results during the wettest years ($\rho = -0.07$, $p = 0.88$). In analogy, we correlated the envelope abundance during the wettest (driest) years and the summer season precipitation amounts for the study region at the southeastern TP (20°-40°N/92°-98°E). In both cases, we obtained insignificant negative relations (wet: $\rho = -0.49$, $p = 0.22$ /dry: $\rho = -0.46$, $p = 0.26$). Generally, negative associations contradict our assumption that an increase in the abundance of envelopes induces an increase in baroclinic instability that initiates low-level cyclogenies and thus wetter conditions. We extended our analyses and conducted the same correlation analyses between the envelope abundance over the entire northern hemisphere (20°-40°N/180°W-180°E), our study area at the southeastern TP, and the summer season precipitation amounts during 1968-2010. Again, insignificant associations confirm that envelopes do not significantly determine the moisture variability at the southeastern TP (northern hemisphere: $\rho = -0.0007$, $p=0.99$/ southeastern TP: $\rho = 0.16$, $p = 0.30$). As a consequence, we assume that upper-tropospheric oscillations induce trough-ridges sequences which determine the envelope development. To capture trough-ridge sequences we examined the geopotential field in 250hPa.

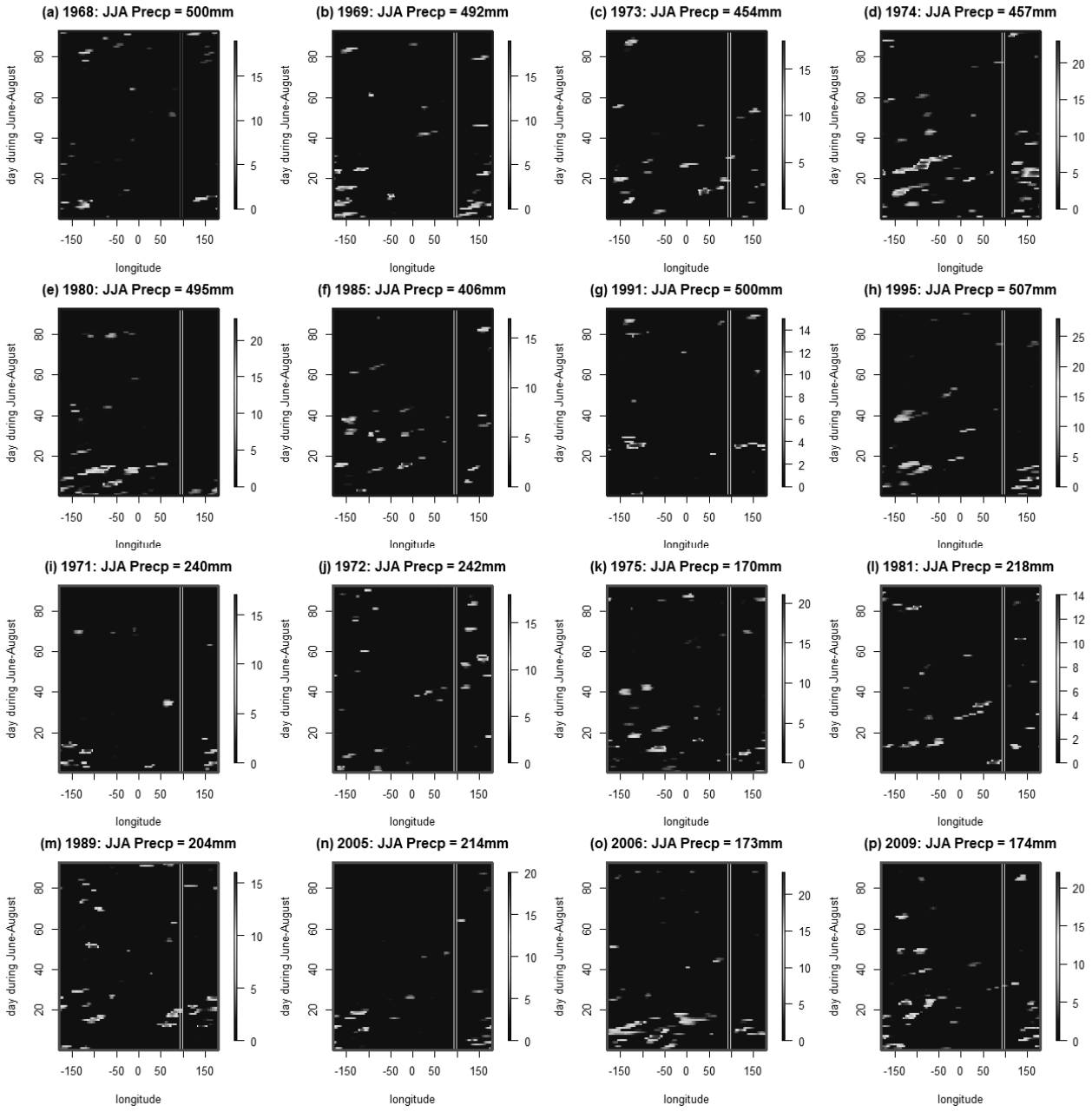

Figure 2: Hovmöller diagrams of spatio-temporal envelope propagation during the summer season (June-August; y-axis represents days of the summer season, with '1' as the 1st of June and '92' as the 31st of August) during years with driest (l-p) and wettest (a-h) summers at study site Bomi, respectively. Gray scale represents the sum of envelopes registered in an area between 20°-40°N at the particular geographical position and time. White lines emphasize the location of the MiMei $\delta^{18}O$ chronology and Bomi climate station location. Envelopes are computed from v-wind data (ERA20C) based on the code of Glatt & Wirth (2014). Summer season precipitation amounts were derived from climate station Bomi.

As displayed in Figure 3, a selection of four dry (a-d) and wet years (e-h) remarkably vary in the position of the geopotential field (bold greyish) line exemplary illustrates the $\phi = 10^5 m^2 s^{-2}$ isohypses). During the years with wetter weather conditions (e-h) distinct troughs or even cold cut-off lows (e) are visible over central Asia (~60°N/~80°E). From a synoptic point of view, these troughs might promote critical relative vorticities, which are supposed to induce cyclogenies. As a consequence, a low pressure system might amplify a northern directed air motion at the low-pressure front and southern directed air motion at its backside. This mechanism seems valid for the study site on the TP (black dot marks the MiMei location), where the distinct backside

characteristic is emphasized by upper tropospheric v-wind velocities >10m/s (meridional directed wind shown as dotted regions north of MiMei). Hence, moist labile air masses are supposed to deeply penetrate at the frontside of this low pressure system onto the TP. On the other hand, a comparable air motion in the upper troposphere over the southeastern TP is not obvious during the exemplarily illustrated dry years, respectively.

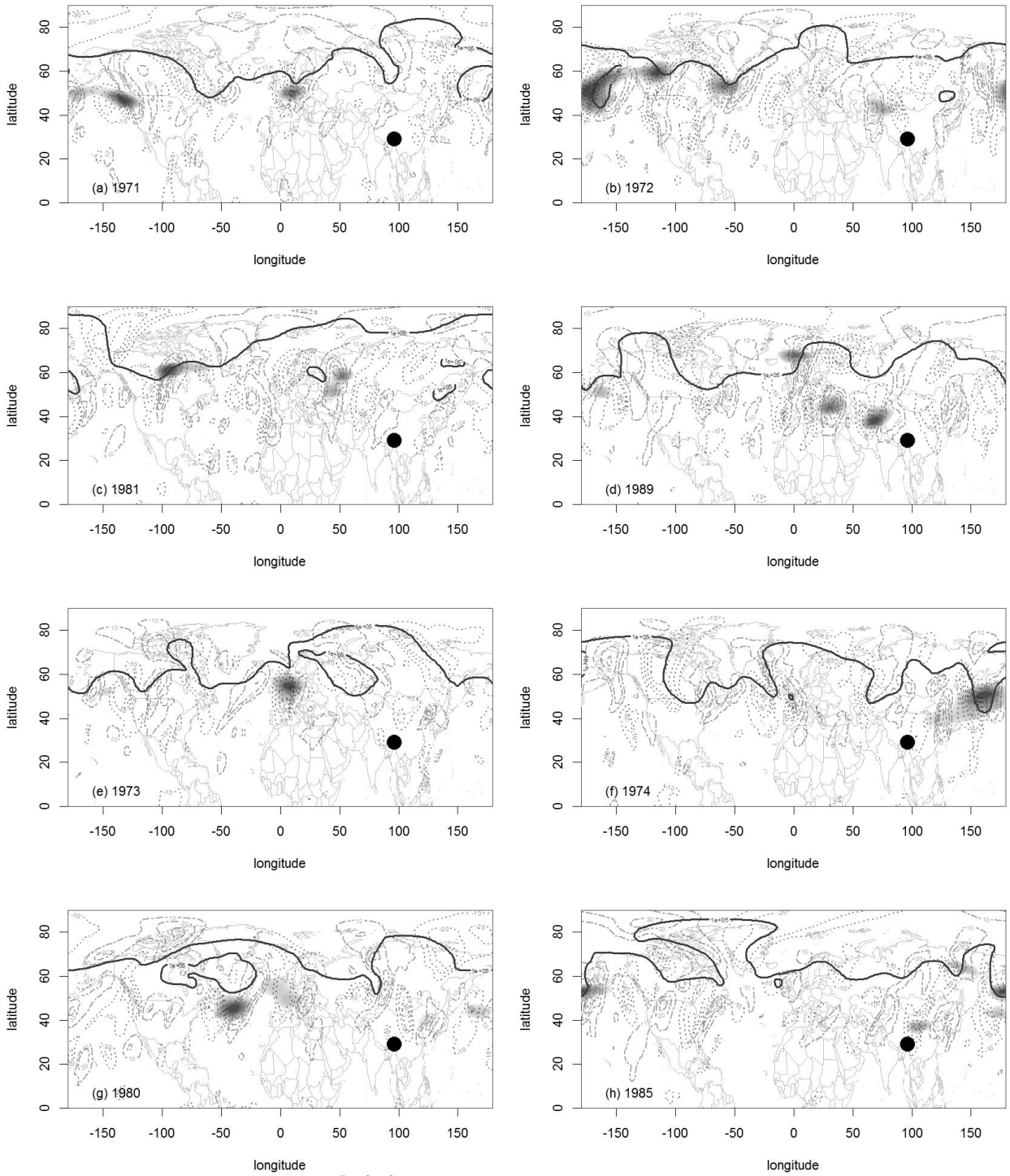

Figure 3: Global position of φ = $10^5 m^2 s^{-2}$ isohypsis (bold solid line) together with the meridional wind field in 250hPa (dashed (S-N directed) and dotted (N-S directed) lines) and accompanied envelopes (gray shaded areas). Black dot marks the location of study site MiMei. The selected years (a-d)represent very dry and (e-h) very wet years at study site MiMei (summer season precipitation amounts please see Figure 2) . Data source: ERA20C.

Instead, a distinct 'Mediterranean-type' waveguide (definition by Bothe et al. 2009) with embedded envelopes is clearly visible. Yet, we have no explanation for below average summer season precipitation amounts in 1989, since Bothe et al. (2009, 2011) and Zhu et al. 2011 actually associated this Mediterranean wave train pattern with extreme wet conditions over the TP, and not with dry conditions. Furthermore, we applied Pearson's correlations to unravel associations between geopotential heights variations extracted for the MiMei study site, summer season precipitation amounts from Bomi, and the MiMei tree-ring $\delta^{18}O$ record (Figure 4). We found a significant negative correlation between summer season precipitation amounts registered at climate station Bomi and the geopotential ϕ (r = -0.27, p = 0.08). Unfortunately, a similar association was not confirmed for the correlation of ϕ and $\delta^{18}O$. It is very likely that other processes (e.g. temperature, relative humidity, cloudiness) superimpose a distinct ϕ-signal in tree-ring $\delta^{18}O$ values. However, to some extent Figure 4 (b) reveals similar trends, particularly since the 1990s. The latter period infers a significant association in the regression line slopes of ϕ and $\delta^{18}O$ ($H_0 : \beta_1 = \beta_2, p = 0.51$). Hence, an increase in ϕ is accompanied by higher $\delta^{18}O$ values, which is clearly related to a drying trend since ~1990s (Figure 4 (a)). These findings suggest a recent frequency increase in southward excursion of the geopotential field from higher latitudes. In this case, 'Scandinavian- wave trains' are likely to induce upper tropospheric high-pressure systems, which prevent a northern propagation of moist labile air masses onto the TP (Bothe et al. 2009). However, the rise in global mean temperatures is supposed to induce a shift of the polar-front northwards (Trouet et al., 2009), leading to lowered ϕ-values further north. Thus, we can currently only speculate that the meander structure of the geopotential field shows stronger amplitudes since ~1990s. However, this issue is beyond the scope of this study and should be addressed in future research efforts.

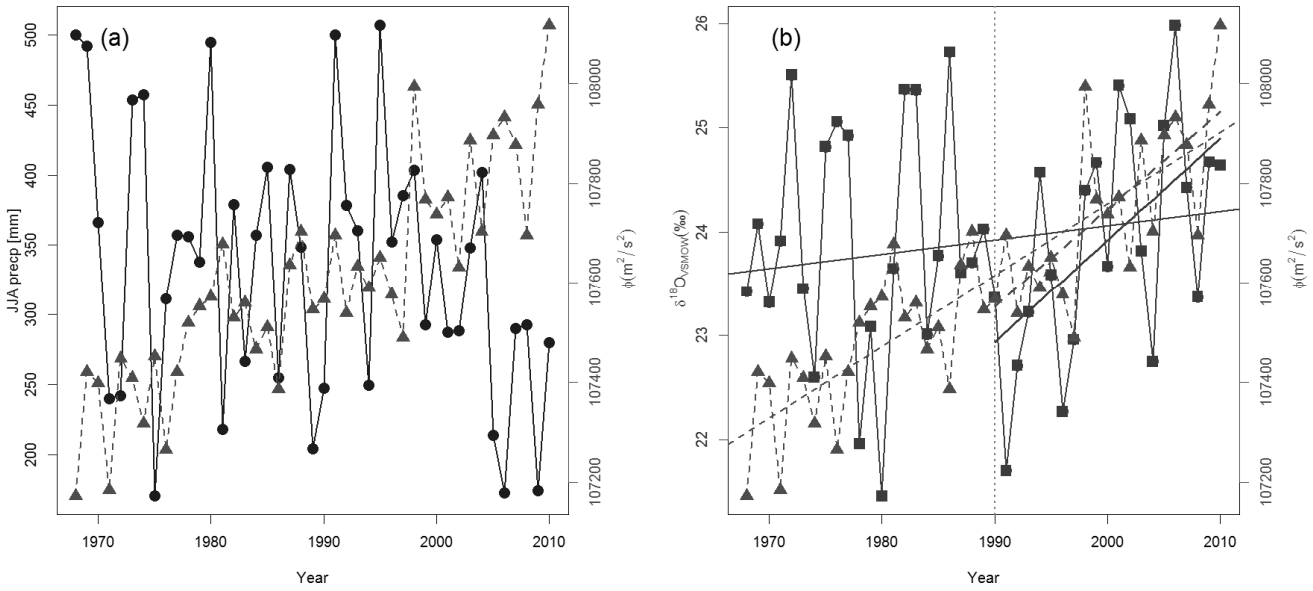

Figure 4: Summer season precipitation amounts (bold line in (a)) and tree-ring $\delta^{18}O$ variability (bold line in (b)) against the geopotential time series (dashed lines) extracted for MiMei (φ [m^2s^{-2}], 250hPa, data source: ERA20C). Additionally displayed in (b) are the trends for φ and $\delta^{18}O$ of the whole period and since 1990 (vertical dashed line marks 1990).

Conclusions

In this study we further tested a hypothesis developed in Wernicke et al. 2017, who speculated that a recent trend of reduced summer moisture on the southeastern TP is induced by frequency increase of westerly wave trains. In order to capture these wave trains, we applied a Hilbert transformation algorithm on the v-wind field in 250hPa. Our findings could not confirm a frequency increase nor decrease in the wave train activity and accompanied humidity variability in the study region on the southeastern TP. The same holds for the most severe dry (wet) summer seasons during 1968-2010. From these findings, we conclude that the geopotential height field configuration and accompanied polar-front position, induces sever dry (wet) summer season condition on the TP. Interestingly, we found significant associations between the summer season precipitation amounts and ϕ. Moreover, the most recent part of a tree-ring based $\delta^{18}O$ chronology widely coincides with the ϕ variability. Hence, to a certain extent, large scale atmospheric dynamics of upper tropospheric processes are detectable in tree-ring archives. This implies that upper tropospheric dynamics can potentially be reconstructed from tree-ring archives and as a consequence the explanatory power of climate response analyses in tree-ring archives can be improved.

Acknowledgements

We express our gratitude to the team of Theoretical Meteorology and Atmospheric Physics from the University of Mainz. Thanks to Prof. Volkmar Wirth and Dr. Joachim Eichhorn for sharing their code and a very friendly communication.

References

Bothe, O., Fraedrich, K., Zhu, X., 2009. The large-scale circulations and summer drought and wetness on the Tibetan plateau. International Journal of Climatology 30, 844-855, doi:10.1002/joc.1946.

Bothe, O., Fraedrich, K., Zhu, X., 2011. Large-scale circulations and Tibetan Plateau summer drought and wetness in a high-resolution climate model. International Journal of Climatology 31, 832{846. doi:10.1002/joc.2124.

Conroy, J.L., Overpeck, J.T., 2011. Regionalization of Present-Day Precipitation in the Greater Monsoon Region of Asia. Journal of Climate 24, 4073-4095. doi:10.1175/2011JCLI4033.1.

Ding, Q., Wang, B., 2005. Circumglobal teleconnection in the northern hemi- sphere summer. Journal of climate 18, 3483-3505. doi:10.1175/jcli3473.1.

Glatt, I., Wirth, V. 2014. Identifying Rossby wave trains and quantifying their properties. Quarerly Jorunal of the Royal Meteorological Society 140, 384-396. doi: 10.1002/qj.2139.

Joseph, P.V., Srinivasan, J., 1999. Rossby waves in May and the Indian summer monsoon rainfall. Tellus A 51, 854-864. doi:10.3402/tellusa.v51i5.14497.

Leyer, I., Wesche, K., 2007. Multivariate Statistik in der Okologie. Springer Berlin Heidelberg. doi:10.1007/978-3-540-37706-1.

Liu, X., Zeng, X., Leavitt, S., Wang, W., An, W., Xu, G., Sun, W., Wang, Y., Qin, D. Ren, J., 2013. A 400-year tree-ring $\delta^{18}O$ chronology for the southeastern Tibetan Plateau: Implications for inferring variations of the regional hydroclimate. Global and Planetary Change 104, 23-33. doi:10.1016/j.gloplacha.2013.02.005.

Ma, J., Yu, J.Y., 2014. Paradox in South Asian summer mon- soon circulation change: Lower tropospheric strengthening and upper tropospheric weakening. Geophysical Research Letters 41, 2934-2940. doi:10.1002/2014GL059891.

Maussion, F., Scherer, D., Mölg, T., Collier, E., Curio, J., Finkelnburg, R., 2014. Precipitation seasonality and variability over the Tibetan Plateau as resolved by the High Asia Reanalysis. Journal of Climate 27, 1910-1927. doi:10.1175/JCLI-D-13-00282.1.

Mölg, T., Maussion, F., Scherer, D., 2014. Mid-latitude westerlies as a driver of glacier variability in monsoonal High Asia. Nature Climate Change 4, 68-73. doi:10.1038/NCLIMATE2055.

Poli, P., Hersbach, H., Tan, D.G.H., Dee, D., Thepaut, J.J., Simmons, A., Peubey, C., Laloyaux, P., Komori, T., Berrisford, P., Dragani, R., Tremolet, Y., Holm, E.V., Bonavita, M., Isaksen, L., Fisher, M., 2013. The data assimilation system and initial performance evaluation of the ECMWF pilot reanalysis of the 20th-century assimilating surface observations only (ERA-20C). Shinfield Park, Reading.

Saeed, S., Müller, W., Hagemann, S., Jacob, D., 2011. Circumglobal wave train and the summer Monsoon over northwestern India and Pakistan: The explicit role of the surface heat low. Climate Dynamics 37, 1045-1060. doi:10.1007/s00382-010-0888-x.

Shi, C., Daux, V., Zhang, Q.B., Risi, C., Hou, S.G., Stievenard, M., Pierre, M., Li, Z., Masson-Delmotte, V., 2012. Reconstruction of southeast Tibetan Plateau summer climate using tree ring $\delta^{18}O$: moisture variability over the past two centuries. Climate of the Past 8, 205-213. doi:10.5194/cp- 8-205-2012.

Trouet, V., Esper, J., Graham, N., Baker, A., Scourse, J., Frank, D., 2009. Persistent positive North Atlantic Oscillation mode dominated the Medieval Climate Anomaly. Science 324, 78-80. doi:10.1126/science.1166349.

Wernicke, J., Hochreuther, P., Grieinger, J., Zhu, H., Wang, L., Bräuning, A., 2015. Hydroclimatic variability of the Tibetan Plateau during the past millennium. Proceedings of the DENDROSYMPOSIUM 2014: May 6th - 10th 15/06. Deutsches GeoForschungsZentrum GFZ. Potsdam. doi:http://doi.org/10.2312/GFZ.b103-15069.

Wernicke, J., Hochreuther, P., Grießinger, J., Zhu, H., Wang, L., Bräuning, A., 2017. Multi-century humidity reconstructions from the southeast- ern Tibetan Plateau inferred from tree-ring $\delta^{18}O$. Global and Planetary Change 149, 26-35. doi:10.1016/j.gloplacha.2016.12.013.

Wolf, G., Wirth, V., 2015. Implications of the Semigeostrophic Nature of Rossby Waves for Rossby Wave Packet Detection. Mon. Wea. Rev. 143, 26-38. doi:10.1175/mwr-d-14-00120.1.

Zhu, X., Bothe, O., Fraedrich, K., 2011. Summer atmospheric bridg- ing between Europe and East Asia: Influences on drought and wetness on the Tibetan Plateau. Quaternary International 236, 151-157. URL: http://dx.doi.org/10.1016/j.quaint.2010.06.015, doi:10.1016/j.quaint.2010.06.015.

Zimin, A.V., Szunyogh, I., Patil, D.J., Hunt, B.R., Ott, E., 2003. Extracting Envelopes of Rossby Wave Packets. Mon. Wea. Rev. 131, 1011-1017. doi:10.1175/1520-0493(2003)131<1011:eeorwp>2.0.co;2.

Exploring stable carbon isotopes in Siberian tree-rings as a potential indicator of precipitation changes after major volcanic eruptions

O.V. Churakova (Sidorova)[1,2], S. Guillet[1], M. Saurer[3,4], Ch. Corona[5], R. Siegwolf[3,4], M. Fonti[2],V. Myglan[2], E. Vaganov[2,6] & M. Stoffel[1]

[1]Institute for Environmental Sciences, University of Geneva, 1205 Geneva, Switzerland
[2]Siberian Federal University, 660049 Krasnoyarsk, Russia
[3]Swiss Federal Institute for Forest, Snow and Landscape Research WSL, 8903 Birmensdorf, Switzerland
[4]Paul Scherrer Institute, 5232 Villigen - PSI, Switzerland
[5]Université Clermont-Auvergne, Geolab, UMR 6042 CNRS, 4 rue Ledru, F-63057 Clermont-Ferrand, France
[6]V.N. Sukachev Institute of Forest SB RAS, Federal Research Center «Krasnoyarsk Science Center SB RAS» 660036 Krasnoyarsk, Russia
E-mail: olga.churakova@hotmail.com

Introduction

Stratospheric sulphate aerosols originating from large explosive volcanic eruptions can have far-reaching impacts on radiation budget, atmospheric and surface temperatures, as well as regional weather patterns, thereby resulting in climatic changes across the globe. Such eruptions also cause changes in atmospheric chemistry, including environmentally important effects such as global ozone depletion (Robock 2000).

Strong surface cooling is known to have occured after some stratospheric Common Era (CE) volcanic eruptions (i.e. CE 536 - unknown, 1257 - Samalas, 1453 - unknown, 1600 - Huaynaputina, 1815 – Tambora and 1991 - Pinatubo) Values in the range of 0.6°C to 1.3°C, in terms of the global average response, have been reported; e.g. Robock (2000), Zielinski et al. (2000); Stoffel et al. (2015); Guillet et al. (2017) or Esper et al. (2017). Data from both climate simulations and temperature-sensitive tree-ring widths and latewood density chronologies have contributed to these estimates. In addition, climate simulation models suggest that a reduction in precipitation can occur over Europe and Siberia in response to large explosive eruptions (Robock & Liu 1994, Wegmann et al. 2014). However, little is known about precipitation changes in the aftermath of these volcanic events from natural archives such as tree ring growth proxies (ring widths and density) because at higher latitude sites tree growth tends to be most strongly temperature controlledHowever, water availability is very important for Siberian trees growing under extreme climate conditions with hot summers and cold winters and tree sensitivity to precipitation may be recorded in other tree ring variables, such as the stable isotope ratios of carbon in tree ring cellulose.

To reveal the influence of water availability as a result of the impact of climate on photosynthesis, carbon isotopes recorded in tree-ring cellulose may help (Farquhar et al. 1989).

In this work, we aim to derive information about precipitation changes after major volcanic eruptions from δ^{13}C tree-ring cellulose chronologies from high-latitude Siberian regions.

Here we explore whether information about precipitation changes after major volcanic eruptions can be elucidated from stable carbon isotope ratios (δ^{13}C) in tree-ring cellulose chronologies from high-latitude larch trees. Water availability strongly controls tree ring δ^{13}C in regions with hot, continental summers by virtue of the climatic response of photosynthetic rate and stomatal conductance (Farquhar et al. 1989).

Material and methods

Study sites

Our study sites are located in the northeastern Yakutia (YAK) [69°N, 148°E], eastern Taimyr (TAY) [70°N, 103°E] and Altai (ALT) [50°N, 89°E]. Larch trees (*Larix cajanderi* Mayr) in YAK, (*Larix gmelinii* Rupr.) in TAY, (*Larix sibirica*) in ALT are long-living trees, growing in the permafrost zone under low annual temperature (-12 - 13°C) and low amount of precipitation (up to 200 mm/year). The permafrost water resource plays an important role in the growth of Siberian trees, where it can both buffer the continental climate and provide an additional water source (Boike et al. 2013). However, this is not always effective for trees from the northern Siberian regions sampled here being unavailable for shallow rooted species, or comprised of waters too cold for uptake (Churakova (Sidorova) et al. 2016). The vegetation period is rather short at these sites, around 90 days based on a growth threshold of +3º C (Körner 2015). Larch trees growing in YAK can live as long as 1216 years (Sidorova et al. 2005), while in TAY according to the findings – ages up to 840 years are possible (Sidorova et al. 2005). Additionally, dead trees are well preserved in the landscape and can be used to extend the chronologies back in time (Sidorova et al. 2005). Monthly climatic data are available from the local weather stations close to the study sites: YAK, TAY, ALT (http://aisori.meteo.ru/ClimateR) for the period 1959-2004. Grid data were not used due to low representativeness from 1900 to 1945.

Tree-ring width analysis

Tree ring data from years characterized by major volcanic eruptions in CE 536, 1257, 1453, 1600, 1815, and 1991 were selected from our chronologies. These eruptions years are identified based on sulfate and sulfur concentration records measured in Greenland and Antarctica ice cores (Sigl et al. 2015). The selected Common Era volcanic years were found in the earlier tree-ring width chronologies of larch from the study sites YAK (Hughes et al. 1999; Sidorova 2003), eastern Taimyr (TAY) (Naurzbaev et al. 2002) and Altai (ALT) (Myglan et al. 2009). The data within these chronologies are tree-ring widths measured from sampled stem discs using the semi-automatic device LINTAB V-3.0 (RinnTech GmbH, Germany) to a ring width precision of 0.01 mm. In a subsequent step, the tree-ring series was cross-dated, and an exact calendar date was determined for each tree ring (Schweingruber et al. 1996; Cook and Krusic 2008). The above papers can be referred to for precise ring width chronology construction information.

Stable carbon isotope analysis

The original stem discs sampled for ring width analysis were sub-sampled, for the CE volcanic years identified above, in order to carry out stable isotope analysis. From the selected, cross-dated sub-samples, we then excluded the first 30 years of each tree sample to avoid the influence of juvenile growth and then selected ± 10 years before and after the volcanic events. Four tree samples for stable carbon isotope analyses, as usual with standards of replication commonly used for these variables (Loader et al. 1997; Sidorova et al. 2008).

Once the relevant sub samples for the $\delta^{13}C$ analysis were identified, standard stable isotope methodologies for wood samples were followed. After splitting the annual rings with a scalpel, the entire wood sample was enclosed in filter bags and an α-cellulose extraction was performed according to the method described by Loader et al. (2007). Stable isotope analysis was conducted at the Paul Scherrer Institute (PSI), Villigen, Switzerland. For the analysis of the $^{13}C/^{12}C$ 0.2-0.3 mg of cellulose for each annual ring was weighed into tin capsules. The carbon isotopic ratios in tree ring cellulose were determined by combustion under oxygen excess at a reactor temperature of 1020ºC with an isotope ratio mass spectrometer delta-S (Finnigan MAT, Bremen, Germany) linked to an elemental analyzer (EA-1110 Carlo Erba, Italy) via a variable open split interface (CONFLO-II, Finnigan MAT, Bremen, Germany). The isotopic values were expressed in the delta notation relative

to the international standard VPDB: $\delta^{13}C_{sample}$ = ($R_{sample}/R_{standard}$-1)•1000, where R_{sample} is the molar fraction of $^{13}C/^{12}C$. The precision is $\sigma \pm 0.1‰$.
The $\delta^{13}C$ cellulose data were corrected for changes in the $\delta^{13}C$ of atmospheric CO_2 in industrial times (Francey et al. 1999, http://www.cmdl.noaa.gov./info/ftpdata.html) from 1800 to present time.

Stable isotope theory

Carbon isotopic ratios in climate sensitive tree rings reflect signals of water availability and air humidity as a result of the climate sensitivity of photosynthetic rate and stomatal conductance. During photosynthesis, several CO_2 fractionation steps take place, first when CO_2 from the atmosphere diffuses through the stomatal pores into the intercellular spaces, and second during CO_2-fixation by the enzyme Rubisco (in the C3 pathway used by common tree species). The opening and closing of the stomatal pore, also in response to climatic demands, balances water loss with the need for CO_2 gain. Under dry conditions, in isohydric species (Körner 2015) such as *Larix* species) the stomata close to conserve water, while under wet conditions the stomata open up to optimize CO_2 assimilation. This process is one end of the carbon isotope-climate system. At the other end of the scale changes in photosynthetic assimilation rate also influence the intercellular CO_2 concentration (c_i) within the leaf spaces by raising or lowering the rate at which CO_2 is utilized to form sugars. Thus increases and decreases in these two rates (stomatal conductance and photosynthetic assimilation) in response to climate ultimately control internal CO_2 partial pressure (c_i) and thus the $\delta^{13}C$ of photosynthate (Farquhar et al. 1989). Plants, through the fractionation set points, discriminate strongly against ^{13}C under conditions of high c_i (when stomata are open or photosynthetic assimilation rate is low) and less strongly as c_i drops (as stomata close or photosynthetic assimilation rate increases) As trees respond to limited water resources, particularly under low amounts of precipitation and relatively warm and dry conditions by reducing the stomatal conductance and photosynthetic rate, this results in a diminished intercellular CO_2 concentration and thus higher stable carbon isotope values (Saurer et al. 2004).
At these strongly continental sites we would interpret stable isotope theory to hypothesize that, in summer when the majority of the photosynthate is laid down in the short growing season, the stable isotope-climate system here will be one of strong stomatal control of ci and thus ca. Stomatal limitation of incoming CO_2 would thus result, we expect, in strong correlations between tree ring $\delta^{13}C$ and hydroclimate variables (precipitation) (Churakova (Sidorova) et al. 2014).

Statistical analysis

Standard response functions were carried out to explore the correlations between the tree ring stable carbon isotope data and local climate data over the available instrumental period, in order to test the above hypothesis. Person's correlation coefficients were calculated between $\delta^{13}C$ in tree-ring cellulose and meteorological data from September of the previous year to August of the current year for the common period from 1966 to 2000.

Results and Discussion

Correlation profiles for the recent 1966-2000 period reveal statistically significant ($p<0.05$) negative correlation coefficients between July precipitation and stable isotope tree ring cellulose chronologies for all study sites, particularly for the high-latitude sites YAK and TAY (Fig. 1a-c, left panel).

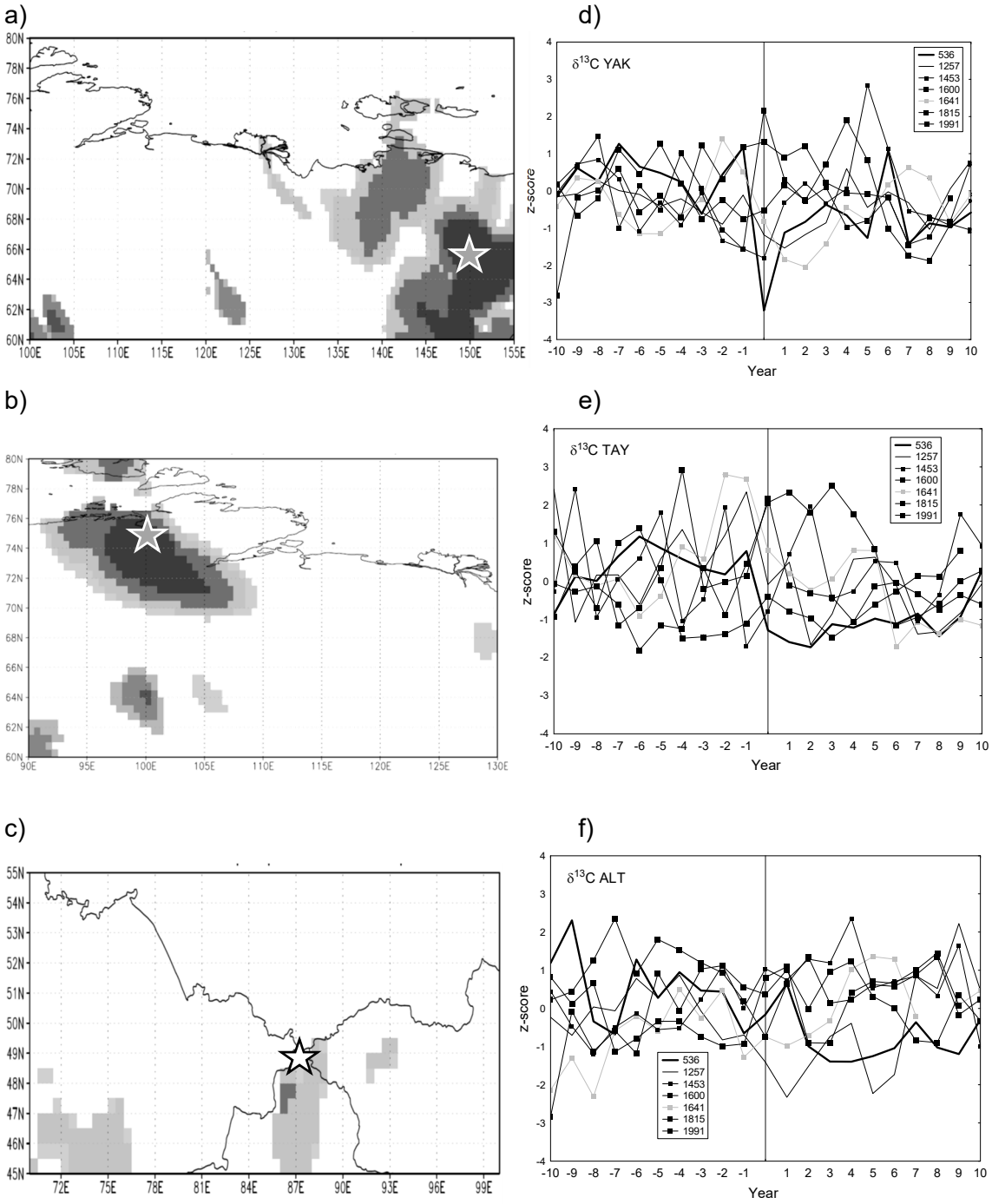

Figure 1: Map of the spatial distribution of the correlations between the $\delta^{13}C$ chronologies and July precipitation during calibration period (1950-2000) for northeastern Yakutia (YAK), eastern Taimyr (TAY) and Russian Altai (ALT). In grey color, we present correlation coefficients in the range between -0.2 and -0.4, whereas dark grey is giving values in the range of -0.5 to -0.7. Location of the study sites are marked with stars. $\delta^{13}C$ in larch tree-ring cellulose chronologies is given for the ten years before and after the largest volcanic eruptions in CE (536, 1257, 1453, 1600, 1641, 1815 and 1991).

The carbon isotope response after the volcanic eruptions was quite variable depending on sites and volcanic events.

Based on the classical carbon isotope fractionation theory (Farquhar et al. 1989), we interpret depletion of ^{13}C as increasing drought conditions after large volcanic eruptions in CE 1258, 1259 for YAK, TAY and ALT (Fig, 1d-f, right panel); 1453, 1642 for YAK (Fig. 1d) and ALT (Fig. 1f); 1991 for ALT (Fig. 1f). The significant decrease in $\delta^{13}C$ values indicating a reduction of photosynthetic activity or an increase in stomatal conductance is due to cold conditions with low vapor pressure deficit

(VPD) during the growing season. This process is strongly enhanced by light reduction, probably due to dust veils (Churakova (Sidorova et al. 2014)). Shifts to wetter environmental changes were detected after Tambora eruption in TAY during summer 1815 and 1816 (Fig. 1e), at dry conditions in ALT during summer of 1817 (Fig. 1f). The summer of 1992 was most likely wet in ALT compared to dry 1991, which was confirmed by the stable isotope chronologies.

The $\delta^{13}C$ of cellulose chronologies constructed for YAK, TAY and ALT sites show differences in absolute values (per mil, data not shown) and standard deviation due to their locations and water source availability for trees. $\delta^{13}C$ chronology from ALT indicates driest conditions when compared to TAY and YAK. Dry conditions cause stomatal closure and lead to low isotopic fractionation that as confirmed in our chronologies. Differences in carbon assimilation rates of trees between sites/regions/latitudes can be explained by the differences in dust veil intensities and in atmospheric circulation patterns, resulting in different light intensities and cloud cover conditions. Reduced light intensity, as produced by a volcanic dust veil, can reduce photosynthesis, which will lead to an increase in the leaf intercellular CO_2 concentration (c_i). Thus $\delta^{13}C$ will decrease accordingly (Farquhar et al. 1989). If we take reduced $\delta^{13}C$ as an indication of stress of the trees, we can infer stressed growth conditions at Siberian study sites.

We conclude that Siberian larch trees exposed to insufficient water availability after CE 536, 541, 1257, 1641 are suffering from drought stress. Heterogeneity in precipitation patterns and volcanic events were found in CE 1453, 1458, 1815 and 1991. Yet, most recent volcanic eruptions occurred in CE 1815, 1991 leading to wetter conditions compared to the first half of the millennia. The carbon isotope patterns provide therefore novel information on the diverse hydrological changes after volcanic eruptions.

Acknowledgements

This work was supported by Marie Curie International Incoming Fellowship (EU_ISOTREC 235122), Era.Net RUSplus project ELVECS (SNF IZRPZ0_164735, RFBR 16-55-76012 Era-a).

References

Boike, J., Kattenstroth, B., Abramova, K. (2013) Baseline characteristics of climate, permafrost and land cover from a new permafrost observatory in the Lena River Delta, Siberia (1998-2011). *Biogeosciences* 10: 2105-2128.

Churakova, (Sidorova) O.V.**,** Bryukhanova, M., Saurer, M., Boettger, T., Naurzbaev, M., Myglan, V.S., Vaganov, E.A., Hughes, M.K., Siegwolf, R.T.W. (2014): A cluster of stratospheric volcanic eruptions in the AD 530s recorded in Siberian tree rings. *Global and Planetary Change* 122: 140-150.

Cook, E.R. & Krusic, P.J. (2008) A Tree-Ring Standardization Program Based on Detrending and Autoregressive Time Series Modeling, with Interactive Graphics (ARSTAN). (ed. by E.R. Cook and P.J. Krusic).

Esper, J., Büntgen, U., Hartl-Meier, C., Oppenheimer, C., Schneider, L. (2017): Northern Hemisphere temperature anomalies during 1450s period of ambiguous volcanic forcing. *Bull. Volcanol.* 79:41.

Farquhar, G.D., Ehleringer, J.R., Hubick, K.T. *Annu. Rev. Plant Physiol. Plant Mol. Biol.* 40: 503 (1989).

Fonti, P., Bryukhanova, M.V., Myglan, V.S., Kirdyanov, A.V., Naumova, O.V., Vaganov, E.A. (2013): Temperature-induced responses of xylem structure of Larix sibirica (Pinaceae) from Russian Altay. *American Journal of Botany* 100(7): 1-12.

Francey, R.J., Allison, C.E., Etheridge, D.M. (1999): A 1000-year high precision record of $\delta^{13}C$ in atmospheric CO_2. *Tellus* 51:170-193.

Guillet, S., Corona, C., Stoffel, M., Khodri, M., Lavigne, F., Ortega, P., Eckert, N., Selenniou, P., Daux, V., Churakova (Sidorova), O.V., et al. (2017): Climate response to the 1257 Samalas eruption revealed by proxy records. *Nature geoscience.* doi:10.1038/ngeo2875.

Körner, C. (2015): Paradigm shift in plant growth control. *Curr Opin Plant Biol* 25:107-114.

Loader, N.J., Robertson, I., Barker, A.C., Switsur, V.R., Waterhouse, J.S. 1997. Improved technique for the batch processing of small whole wood samples to alpha-cellulose. *Chemical Geology*. 136: 313-317.

Myglan VS, Oidupaa O Ch, Kirdyanov AV, Vaganov EA (2008) 1929-year tree-ring chronology for Altai-Sayan region (Western Tuva). Journal of archeology, ethnography and anthropology of Eurasia 4 (36), 25-31.

Naurzbaev, M.M., Vaganov, E.A., Sidorova, O.V., Schweingruber, F.H. 2002. Summer temperatures in eastern Taimyr inferred from a 2427-year late-Holocene tree-ring chronology and earlier floating series. *The Holocene.* 12(6): 727-736.

Robock, A. (2000): Volcanic eruptions and climate. *Reviews of Geophysics*. 38(2): 191-219.

Robock, A., Mao, J. (1992): Winter warming from large volcanic eruptions. *Geophysical Research Letters*. 19: 2405-2408.

Schweingruber, F.H. *Tree rings and environment dendroecology* (Paul Haupt Publ Bern, Stuttgart, Vienna 1996), pp. 609.

Sigl M, Winstrup M, McConnell JR et al. (2015) Timing and climate forcing of volcanic eruptions for the past 2500 years. Nature 523:543-549. Doi:10.1038/nature14565.

Stoffel, M., Khodri, M., Corona, C., Guillet, S., Poulain, V., Bekki, S., Guiot, J., Luckman, B.H., Oppenheimer, C., Lebas, N., Beniston, M., Masson-Delmotte, V. (2015): Estimates of volcanic-induced cooling in the Northern Hemisphere over the past 1,500 years. *Nature Geoscience* 8: 784–788.

Wegmann, M., Bronnimann., S, Bhend, J, Franke J, Folini D, Wild M, Luterbacher J (2014) Volcanic influence on European summer precipitation through monsoons: possible cause for “Years without Summer”. J Clim 27:3683–3691Sugimoto et al. 2002; Boike et al. 2013; Saurer et al. 2016

Zielinski, G.A., Mayewski, P.A., Meeker, L.D., Whitlow, S., Twickler, M.S., *et al.* (1994): Record of volcanism since 7000 BC from the GISP2 Greenland ice core implications for the volcano-climate system. *Science* 264 (5161): 948-952.

Long-term oxygen isotope chronologies from a Mediterranean island

S. Szymczak[1], A. Bräuning[1] & M. Joachimski[2]

[1]Institute of Geography, FAU Erlangen-Nuremberg, Wetterkreuz 15, 91058 Erlangen
[2]Geo-Center of Northern Bavaria, FAU Erlangen-Nuremberg, Schlossgarten 5, 91054 Erlangen
E-mail: sonja.szymczak@fau.de

Introduction

Oxygen isotopes are, beside carbon isotopes, the most frequently measured isotopes in tree-ring cellulose. $\delta^{18}O$ of tree-ring cellulose is determined by several factors, e.g. the $\delta^{18}O$ value of source water, enrichment of ^{18}O-isotopes in the leafwater and biochemical fractionations (Helle & Schleser 2004), which in turn are controlled by climate parameters. The isotopic composition of source water is related to temperature, wheras the evaporative enrichment in the leaves is dominantly controlled by air humidity. Oxygen isotopes may therefore preserve a past climate signal and several studies observe high correlations between $\delta^{18}O$ of tree-rings and $\delta^{18}O$ of source water or relative air humidity (e.g. Anderson et al. 1998, Burk & Stuiver 1981, Saurer 2003). On the other hand, oxygen isotope ratios often seem to be more influenced by large scale circulation patterns rather than by a single local acting climate parameter (e.g. Reynolds-Henne et al. 2007) resulting in low correlations with local climate parameters (McCarroll & Loader 2004). Thus, oxygen isotope series can serve as a proxy of past monsoon activity (Grießinger et al. 2011, Li et al. 2011, Shi et al. 2012), ENSO (Liu et al. 2012) or hurricane activity (Mora et al. 2007).
The development of robust climate proxy archives is especially mandatory in regions vulnerable to current climate change, like the Mediterranean area. Oxygen isotope chronologies from these locations are therefore of special interest since the reconstruction of past circulation patterns contributes to a better understanding of current climate change. Accordingly, we developed four annually resolved long-term oxygen isotope chronologies from tree-ring cellulose of *Pinus nigra* for different upper tree line locations on Corsica and analysed regional differences between the isotope chronologies as well as the climate-isotope relationship.

Study site

The mountainous island of Corsica is located in the western part of the Mediterranean basin, an area especially vulnerable to current climate change with more pronounced drought stress during summer months in the coming decades (Giorgi 2006). Beside typical Mediterranean vegetation and climate along the coastline, the interior of the island is characterised by rugged mountain ranges and hosts alpine floristic elements and climate characteristics, like a continuous snow cover in winter. While temperature is mainly determined by altitude and decreases with a lapse rate of 0.57°C per 100 m (MétéoFrance 2010), precipitation shows a more diverse pattern, with the north-east of the main mountain range being somewhat drier than the west and the south. Mean annual precipitation increases from approximately 600 mm/a along the coast up to nearly 1400 mm/a in 1000 m altitude (MétéoFrance 2010). The mountain forest belt mainly consists of Corsican pine trees (*Pinus nigra* ssp. *laricio*), a subspecies of Black pine (*Pinus nigra*). Several individuals reach ages up to more than 800 years (Szymczak et al. 2014), which are among the oldest living trees found in the Mediterranean.
Trees were sampled at four upper tree line sites in the main mountain range (Fig. 1). Asco (1500 m asl) is located in the headwaters of an sheltered east-west striking valley north of Monte Cinto (2706 m asl). Local climate is relatively cold and dry compared to other mountain sites. Ballone is located in a secondary valley of the dry Niolo high valley at the southern slopes of Monte Cinto.

Studied *Pinus nigra* trees (1600-1700 m asl) grow on a steep slope with sparse vegetation cover. Drought stress during summer months is more pronounced than at Asco and the local climate can be characterised as warm and dry. Capannelle (1700 m asl) is located further south on the south-east exposed slopes of Monte Renoso (2352 m asl). Local climate is cold and wet because air masses from the east coast can nearly unhampered reach the study site and fog is very common. Asinao (1350 m asl) is located in the Asinao valley, a northeast-southwest striking valley south of Monte Incudine (2136 m asl). Sampled trees grow on a talus slope consisting of granite blocks on shallow soils with low water-holding capacity.

Material and methods

Old trees (mean ages range from 700 years (site Asco) to 390 years (site Capannelle)) were sampled at the four upper tree line sites. After dating and crossdating the ring-width series tree rings were separated with a scalpel and contemporaneous material from 5-6 trees per site was pooled prior to cellulose extraction. Pooling of several trees reduces the number of samples to be analysed, and the validity of the pooling approach for *P. nigra* was proven by an earlier study (Szymczak et al. 2012). Since cellulose extraction was shown to be an important prerequisite for the development of isotope series from *P. nigra* (Szymczak et al. 2011), α-cellulose was extracted from all samples prior to isotope measurements following the method described in Szymczak et al. (2012).

For oxygen isotope analyses, subsamples of 0.06 – 0.12 mg from each year were weighed into silver capsules. Oxygen isotopes ratios were measured on duplicates using a TC-EA coupled online to a Thermo Delta Plus mass spectrometer. Isotopic compositions are reported in permil using the conventional δ notation relative to VSMOW-standard (Vienna Surface Mean Ocean Water).

Correlations between oxygen isotopes values and climate parameters were calculated with the program DENDROCLIM 2002 (Biondi & Waikul 2004). Since climate records from Corsican mountains are rare and rather short, we used a climate data set for Italy provided by the Tyndall Centre for Climate Change Research (Mitchell et al. 2002). This climate data set gives averages for temperature and precipitation (AD 1901-2000) as well as cloud coverage (AD 1943-2000) based on all Italian climate stations. The data set is representative for Corsican climate supported by strong correlations between climate stations on Corsica and the data set (e.g. r = around 0.6 for precipitation (annual values, period 1977-2000) and r = between 0.4 and 0.9 for temperature (annual values, period 1978-2000)). The mean annual values for temperature and precipitation better represent the mountain climate than do the Corsican coastal stations for which longer records are available (MétéoFrance 2010). The calibration period was restricted to the time period 1951-2000 for temperature and precipitation because the number of climate stations covering the early 50 years is considerably lower. We further calculated correlations between $\delta^{18}O$ values of tree-ring cellulose and $\delta^{18}O$ values of precipitation from the station Genoa, the nearest longer record (1973-1995) available from the GNIP Database (IAEA/WMO 2006). Correlations were calculated over an 18-months period from previous year May to October of the current year, thus including two vegetation periods (May-October) and one vegetation break.

Results

Oxygen isotope chronologies

The four oxygen isotope chronologies are presented in Fig. 1. The longest record, Asco, is characterised by a high variability in the early years (AD 1185-1330) which is due to the lower sample depth (Tab. 1). The period AD 1330-1540 is characterised by constantly high isotope values without strong annual or decadal variations. The highest values occur around AD 1710-1740 and AD 1950-1960. The mean value of the chronology is 32.2‰ with a range of 4.9‰ (Tab. 1). The mean value of the Ballone chronology is slightly higher and the values show a broader

range (Tab. 1). The Ballone chronology reports higher variability on decadal scale, especially in the early years with low sample depth, and is characterised by a decreasing trend over the whole time period. From around AD 1404-1560 the values show a strong decreasing trend and high interannual variability. Afterwards, the values remain relatively stable, followed by a phase with remarkably low values around AD 1800. The most recent years from around AD 1910 onwards are characterised by decreasing values. The oxygen isotope values of both southern chronologies, Asinao and Capannelle, are lower than isotope values from the northern chronologies reflected by lower mean values but variability is comparable (Tab. 1). The Asinao chronology is characterised by decadal fluctuations from around AD 1448-1740, followed by a phase with less decadal variability but a strong decreasing trend. Values reach the absolute minimum around AD 1930-1935 while an increasing trend is observable for the most recent years. The shortest chronology, Capannelle, can be divided into two distinct parts: AD 1582-1760 characterised by high interannual variability and a strong decreasing trend and AD 1760-2010 characterised by low interannual variability, no clear trend and low variability.

Inter-site correlations reveal a maximum value of 0.72 between sites Asinao and Capannelle and a minimum value of 0.32 between Asco and Capannelle (Tab. 2). Ballone shows rather similar correlations with all sites while Asinao and Capannelle are strongly correlated with each other but show lower correlations with the northern sites. Asco is most different from the other sites with all inter-site correlations being low.

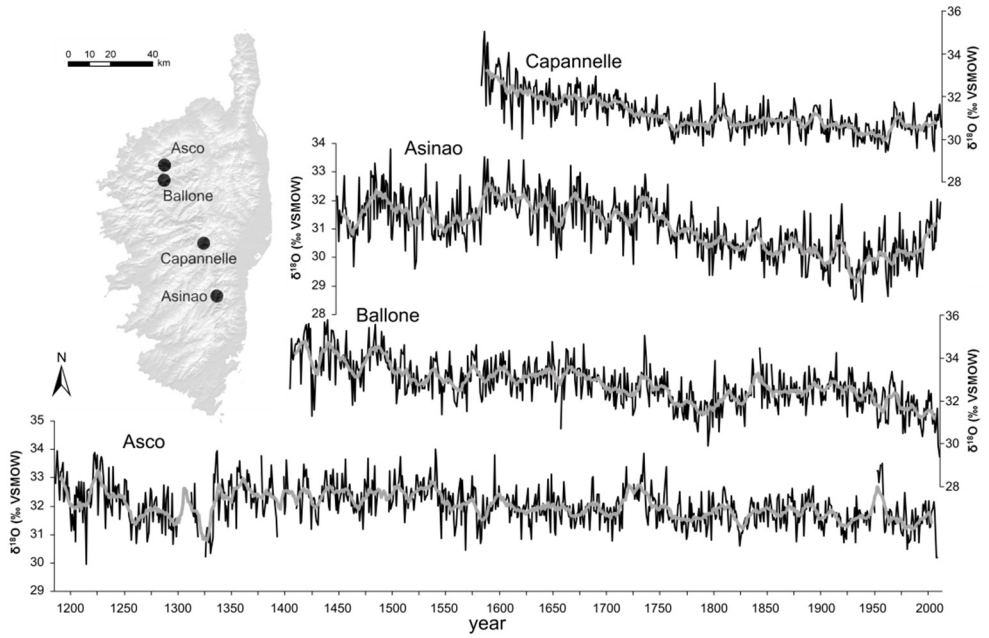

Figure 1: Annually resolved oxygen isotope chronologies for four mountain sites on Corsica. The grey line is an 11-year running mean.

Table 1: Statistical parameters of the oxygen isotope chronologies.

	altitude (m asl)	lat/long	time period	no. of trees	sample depth ≥ 4	mean $\delta^{18}O$ (‰)	range (‰)
Asco	1500	42.24 N, 8.56 E	1185-2008	6	1362-2008	32.2	4.9
Asinao	1350	41.50 N, 9.12 E	1448-2009	6	1655-2009	31.1	5.4
Ballone	1650	42.21 N, 8.54 E	1404-2008	6	1512-2008	32.8	6.4
Capanelle	1700	42.05 N, 9.09 E	1582-2010	5	1586-2010	31.2	5.7

Table 2: Site-by-site correlation matrix calculated over the common time period AD 1582-2008.

	Asinao	Ballone	Capannelle
Asco	0.41	0.48	0.32
Asinao		0.52	0.72
Ballone			0.53

Climate-isotope relationships

The oxygen isotope chronologies show only weak correlations with climate parameters and correlations are rarely significant (Fig. 2). The highest correlations occur with precipitation. All sites except Ballone report stronger correlations with precipitation than with temperature. The highest correlation is -0.36 (Asinao with March precipitation). The dominant precipitation signal at the southern sites is a negative correlation with several months of the vegetation break, which is strongest when regarding the 6-months period October of the previous year to March of the current growth year. Instead, Ballone and Asco show positive correlations with January and DJF-precipitation. Dependency of the oxygen isotope ratios on humidity is further supported by correlations of comparable strength with cloud coverage (Fig. 2). The winter signal is not as strong as observed for precipitation, but it shows the same pattern (negative correlations at Asinao and Capannelle, positive correlations at Asco and Ballone). Most notably, these opposing correlations can be observed for the months DJF. Beside the winter signal, especially the southern study sites show negative correlations with summer cloud coverage. The highest correlation (0.32) is observed between previous May at Asco and previous December at Ballone. The weakest and mainly non-significant correlations are observed for temperature, where no clear pattern is visible. The highest correlation is 0.31 (Asinao with MJJA temperature). High correlations were found with $\delta^{18}O$ of precipitation from Genoa, but it should be kept in mind that the time period used for calculating the relationship is rather short (1973-1995) (Fig. 2). Nevertheless, these correlations underline the complexity of the oxygen isotope signal of our sites, since correlations occur with previous year May and June as well as with winter months and several months of the current vegetation period (Capannelle with JJA).

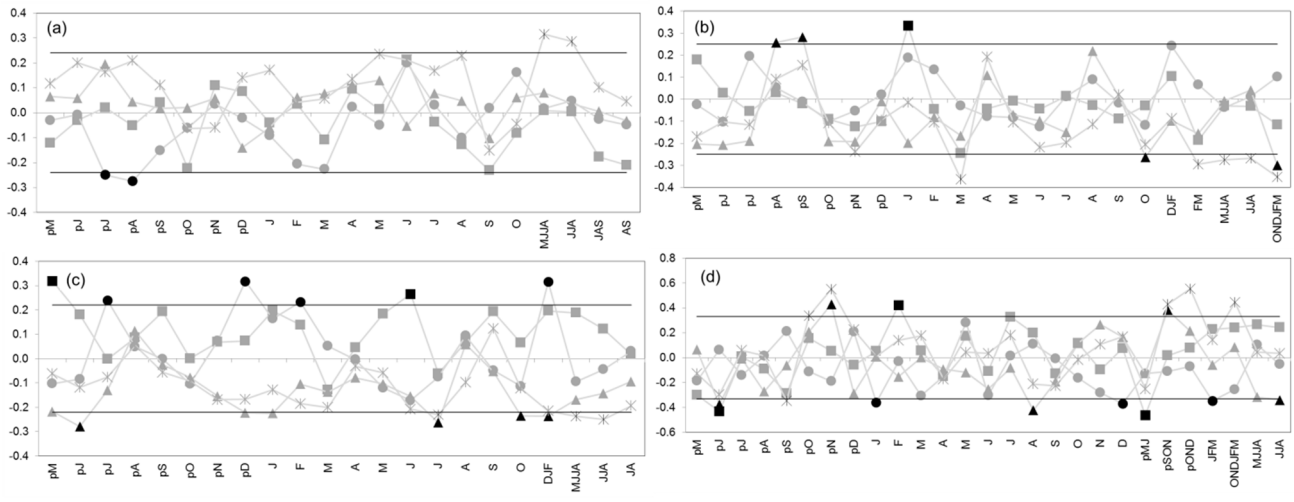

Figure 2: Pearson's correlation coefficients for oxygen isotope ratios of tree-ring cellulose and (a) mean monthly temperatures (time period 1951-2000), (b) monthly precipitation sums (time period 1951-2000), (c) cloud coverage (time period 1943-2000), and (d) $\delta^{18}O$ values of precipitation at Genoa (time period 1973-1995) plotted for an 18-months period from previous May (pM) to October of the current year. Black horizontal lines represent the significance level ($p<0.05$), significant values are marked with black colour. Rectangles: Asco, circles: Ballone, triangles: Capannelle, asterisks: Asinao.

Discussion of climate signal and dependency on $\delta^{18}O$ of precipitation

The low interannual and decadal variability may indicate that the oxygen isotope chronologies rather reflect long-term changes of a regional forcing factor than short-term variations of local climate parameters. The similarities of the high-frequency trends between chronologies from different sites support a main common driving force responsible for oxygen isotope discrimination among the island. Correlations underline the importance of winter precipitation as the main source for refilling the soil water reservoir and providing water for plant metabolism at the beginning of the vegetation period. Cloud coverage and temperature during the vegetation period influence the rate of isotope fractionation due to evapotranspiration (McCarrol & Loader 2004).

Other studies reported strong correlations between oxygen isotope chronologies from tree-ring cellulose and climate parameters, like precipitation (e.g. Battipaglia et al. 2008), temperature (e.g. Loader et al. 2008), sunshine duration (e.g. Kress et al. 2010), or air pressure (Seftigen et al. 2011). A strong precipitation signal can occur where trees grow on a blocky subsurface so that roots cannot reach deeper water reservoirs and trees depend directly on precipitation as water source. In concordance with this theory, a strong precipitation signal in the oxygen isotope series from sites Ballone and Asinao can be expected. However, the highest correlation is 0.37 and thus relatively weak. This may be due to the fact that oxygen isotope values in tree-ring cellulose are influenced by several factors and that values observed in tree-ring cellulose from *P. nigra* reflect a mixture of these different influences.

Other studies from the Mediterranean also report difficulties in extracting climate signals from oxygen isotope chronologies (e.g. Andreu-Hayles et al. 2016, Konter et al. 2014). The weak correlations with climate parameters might indicate that the isotopic signature in tree-ring cellulose strongly depends on the isotopic signature of the local source water. The isotopic signature of precipitation water is not related with precipitation amount; hence a correlation with precipitation amount cannot be established. The amount influences the isotopic signature in tree-ring cellulose only indirect: If the amount of winter precipitation is high, soil water reservoirs can be filled adequately and can be used for plant metabolism in the following vegetation period. Accordingly, the isotopic signature in tree-ring cellulose reflects the isotopic signature of winter precipitation. If the amount of winter precipitation is low, the amount of soil water is limited so that tree growth depends more on summer precipitation during the vegetation period as water source. Accordingly, the isotopic signature in tree-ring cellulose reflects the isotopic signature of summer precipitation.

The isotopic signature of precipitation can be modified in several ways in the mountains of Corsica. Both, the altitudinal and the continental effect in the interior of the mountain range must be taken into account. $\delta^{18}O$ values further differ between different types of precipitation with snow being isotopically more depleted than rain. Further variability is added by the dependency of $\delta^{18}O$ values of precipitation on the origin of the air mass. The Mediterranean is influenced by air masses from different origins throughout the year. During summer months, the Mediterranean is located in the subtropical high pressure belt with air masses originating from the African continent. In contrast, the Mediterranean is located in the west wind zone during winter months and is hence influenced by wet air masses originating from the Atlantic Ocean. Isotope signatures of precipitation can be used to trace the origin of air masses (Rindsberger et al. 1983). The analysis of 12 storm events revealed that rains most depleted in $\delta^{18}O$ are related to air masses coming from North-East Europe, whereas rains most enriched in $\delta^{18}O$ are associated with air masses originating from the Atlantic Ocean (Rindsberger et al. 1983). Celle-Jeanton et al. (2001) reported a unique isotopic signature for the Western Mediterranean Sea, with a value between those of the Eastern Mediterranean basin and the Atlantic Ocean. In our study, the southern sites (Asinao and Capannelle) revealed lower mean $\delta^{18}O$ values than the northern sites (Asco and Ballone). These differences are probably caused by the latitude effect on $\delta^{18}O$ of precipitation which was found to be unusually steep in Corsica, with a value of -1.8‰ per degree latitude (van Geldern et al. 2014).

The authors related the latitude effect to a large contribution of precipitation from subtropical air masses which mostly affect southern Corsica. It is possible that the longer influence of subtropical air masses in southern Corsica leads to lower values of $\delta^{18}O$ in tree-ring cellulose at Asinao and Capannelle.

This high variability of the isotopic signature of local source water makes a climatic interpretation of the $\delta^{18}O$ values from tree-ring cellulose challenging. Further variability is added by the ramified root system of *Pinus nigra* with access to different soil water levels (Stokes et al. 2002). Depending on the water holding capacity of the subsurface, trees can use either soil water reservoirs for water uptake or depend more on summer precipitation in areas with lower water holding capacity. The dependency on the isotopic signature of source water is supported by a comparison with stream water $\delta^{18}O$, which represents the primary isotopic composition of annual precipitation (van Geldern et al. 2014). $\delta^{18}O$ values from the stream Cannereccia, located very close to the tree-ring sampling site Capannelle, are available for four years, sampled in May each year. The z-transformed values reveal a strong coherency between $\delta^{18}O$ values of stream water and $\delta^{18}O$ values of tree-ring cellulose (Fig. 3). Although the time series is rather short, these findings underline the importance of the isotopic signature of precipitation and hence source water on the $\delta^{18}O$ values in tree-ring cellulose from *P. nigra*.

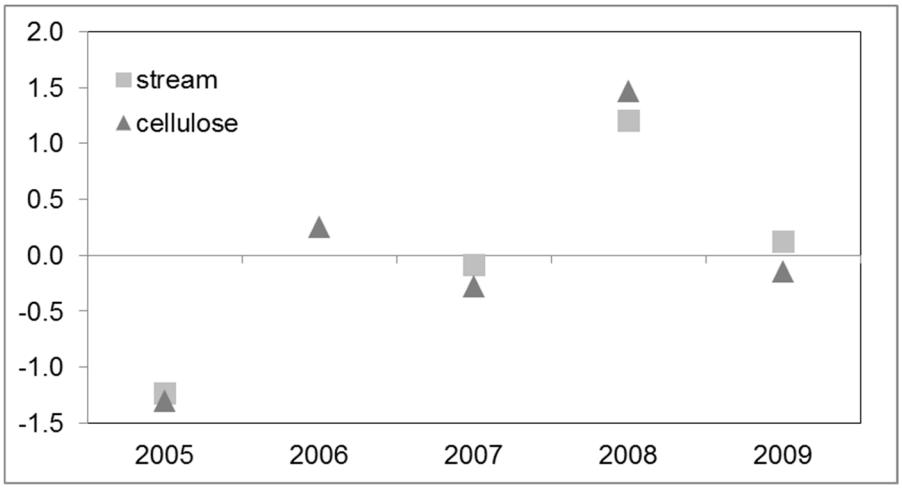

Figure 3: Comparison of $\delta^{18}O$ values of stream water (stream Cannereccia; close to tree ring site Capannelle) and $\delta^{18}O$ values of tree-ring cellulose (site Capannelle). Values are z-transformed for a better comparison. Stream water $\delta^{18}O$ values are from van Geldern et al. (2014).

Conclusions and outlook

The $\delta^{18}O$ signal in tree-ring cellulose from *P. nigra* on the island of Corsica is very complex and is influenced by several factors, which are not yet fully understood. For a thorough interpretation of the oxygen isotope chronologies, the new established project Corsic*Archive* (**A**ltitudinal Gradients and Forest **R**esponse: **C**limate, **H**ydrology and **I**sotope **V**ariability of a Mediterranean **E**cosystem) foresees to measure oxygen isotope ratios in tree-ring cellulose, needle water, xylem water, soil water and precipitation in intra-annual intervals. The superordinate aim of the project is to better understand the processes responsible for spatial and temporal oxygen isotope variability in tree rings and in the hydrological cycle on Corsica.

Acknowledgements

This work was supported by the German Science Foundation for funding the project (JO 219/11-1). Daniele Lutz and Eva-Maria Harth are thanked for help during cellulose extraction and isotope analyses.

References

Anderson, W., Bernasconi, S., McKenzie, J., Saurer, M. (1998): Oxygen and carbon isotopic record of climatic variability in tree ring cellulose (*Picea abies*): an example from central Switzerland (1913-1995). *Journal of Geophysical Research 103(D24)*: 31625-31636.

Andreu-Hayles, L., Ummenhofer, C.C., Barriendos, M., Schleser, G.H., Helle, G., Leuenberger, M., Guitérrez, E., Cook, E.R. (2016): 400 Years of summer hydroclimate from stable isotopes in Iberian trees. *Climate Dynamics 49:* 143-161.

Battipaglia, G., Jäggi, M., Saurer, M., Siegwolf, R.T.W., Cotrufo, M.F. (2008): Climatic sensitivity of $\delta^{18}O$ in the wood and cellulose of tree rings: Results from a mixed stand of *Acer pseudoplatanus* L. and *Fagus sylvatica* L.. *Palaeography, Palaeoclimatology, Palaeoecology 261*: 193-202.

Biondi, F., Waikul, K. (2004): DENDROCLIM2002: a C++ program for statistical calibration of climate signals in tree-ring chronologies. *Computers and Geosciences 30*: 303-311.

Burk, R.W.H., Stuiver, M. (1981): Oxygen isotope ratios in trees reflect mean annual temperature and humidity. *Science 211*: 1417-1419.

Celle-Jeanton, H., Travi, Y., Blavoux, B. (2001): Isotopic typology of the precipitation in the Western Mediterranean region at three different time scales. *Geophysical Research Letters 28(7)*: 1215-1218.

Giorgi, F. (2006): Climate change hot-spots. *Geophysical Research Letters 33*: L08707.

Grießinger, J., Bräuning, A., Helle, G., Thomas, A., Schleser, G. (2011): Late Holocene Asian summer monsoon variability reflected by $\delta^{18}O$ in tree-rings from Tibetan junipers. *Geophysical Research Letters 38*: L03701.

Helle, G., Schleser, G.H. (2004): Interpreting climate proxies from tree-rings. In: Fischer, H., Floeser, G., Kumke, T., Lohmann, G., Miller, H., Negendank, J.F.W., Storch, H. (eds.): The KIHZ project: Towards a synthesis of Holocene proxy data and climate models. Springer, 129-148.

IAEA/WMO (2006): Global Network of Isotopes in Precipitation. The GNIP Database. Accessible at http://www.iaea.org/water (site accessed: 18th May 2012).

Konter, O., Holzkämper, S., Helle, G., Büntgen, U., Saurer, M., Esper, J. (2014): Climate sensitivity and parameter coherency in annually resolved $\delta^{13}C$ and $\delta^{18}O$ from *Pinus uncinata* tree-ring data in the Spanish Pyrenees. *Chemical Geology 377*: 12-19.

Kress, A., Saurer, M., Siegwolf, R.T.W., Frank, D.C., Esper, J., Bugmann, H. (2010): A 350 year drought reconstruction from Alpine tree ring stable isotopes. *Global Biogeochemical Cycles 24 GB2011*.

Li, Q., Nakatsuka, T., Kawamura, K., Liu, Y., Song, H. (2011): Regional hydroclimate and precipitation $\delta^{18}O$ revealed in tree-ring cellulose $\delta^{18}O$ from different tree species in semi-arid Northern China. *Chemical Geology 282*: 19-28.

Liu, X., An, W., Treydte, K., Shao, X., Leavitt, S. Hou, S., Chen, T., Sun, W., Qin, D. (2012): Tree-ring $\delta^{18}O$ in southwestern China linked to variations in regional cloud cover and tropical sea surface temperature. *Chemical Geology 291*: 104-115.

Loader, N.J., Santillo, P.M., Woodman-Ralph, J.P., Rolfe, J.E., Hall, M.A., Gagen, M., Robertson, I., Wilson, R., Froyd, C.A., McCarroll, D. (2008): Multiple stable isotopes from oak trees in southwestern Scotland and the potential for stable isotope dendroclimatology in maritime climatic regions. *Chemical Geology 252*: 62-71.

McCarroll, D., Loader, N.J. (2004): Stable isotopes in tree rings. *Quaternary Science Reviews 23*: 771-801.

Météo-France (2010): Precipitation and temperature records of Météo-France weather stations. Accessible at http://france.meteofrance.com (site accessed 24 February 2010)

Mitchell, T.D., Hulme, M., New, M. (2002): Climate data for political areas. *Area 34*: 109-112.

Mora, C.I., Miller, D.L., Grissino-Mayer, H.D. (2007): Cellulose: Tropical cyclones, droughts and climate oscillations. In: Dawson, T.E., Siegwolf, R.T.W. (eds.): Stable isotopes as indicators of ecological change. Elsevier, 63-75.

Reynolds-Henne, C.E., Siegwolf, R.T.W., Treydte, K., Esper, J., Henne, S., Saurer, M. (2007): Temporal stability of climate-isotope relationships in tree rings of oak and pine (Ticino, Switzerland). *Globel Biogeochemical Cycles 21 GB4009*.

Rindsberger, M., Magaritz, M., Carmi, I., Gilad, D. (1983): The relation between air mass trajectories and the water isotope composition of rain in the mediterranean sea area. *Geophysical Research Letters 10(1)*: 43-46.

Saurer, M. (2003): The influence of climate on the oxygen isotopes in tree rings. *Isotopes in Environmental and Health Studies 39(2)*: 105-112.

Seftigen, K., Linderholm, H.W., Loader, N.J., Liu, Y., Young, G.H.F. (2011): The influence of climate on $^{13}C/^{12}C$ and $^{18}O/^{16}O$ ratios in tree ring cellulose of *Pinus sylvestris* L. growing in the central Scandinavian Mountains. *Chemical Geology 286*: 84-93.

Shi, C., Daux, V., Zhang, Q.-B., Risi, C., Hou, S.-G., Stievenard, M., Pierre, M., Li, Z., Masson-Delmotte, V. (2012): Reconstruction of southeast Tibetan Plateau summer climate using tree ring $\delta^{18}O$: moisture variability over the past two centuries. *Climate of the Past 8*: 205-213.

Stokes, A., Fourcaud, T., Hruska, J., Cermak, J., Nadyezdhina, N., Nadyezhdin, V., Praus, L. (2002): An evaluation of different methods to investigate root system architecture of urban trees *in situ*: I. Ground-penetrating radar. *Journal of Arboriculture 28(1)*: 2-10.

Szymczak, S., Joachimski, M.M., Bräuning, A., Hetzer, T., Kuhlemann, J. (2011): Comparison of whole wood and cellulose carbon and oxygen isotope series from *Pinus nigra* ssp. *laricio* (Corsica/France). *Dendrochronologia 29*: 219-226.

Szymczak, S., Joachimski, M.M., Bräuning, A., Hetzer, T., Kuhlemann, J. (2012): Are pooled tree ring $\delta^{13}C$ and $\delta^{18}O$ series reliable climate archives? – a case study of *Pinus nigra* ssp. *laricio* (Corsica/France). *Chemical Geology 308-309*: 40-49.

Szymczak, S., Hetzer, T., Bräuning, A., Joachimski, M.M., Leuschner, H.-H., Kuhlemann, J. (2014): Combining wood anatomy and stable isotope variations in a 600-year multi-parameter climate reconstruction from Corsican black pine. *Quaternary Science Reviews 101*: 146-158.

van Geldern, R., Kuhlemann, J., Schiebel, R., Taubald, H., Barth, J.A.C. (2014): Stable water isotope patterns in a climate change hotspot: The isotope hydrology framework of Corsica (western Mediterranean). *Isotopes in Environmental and Health Studies 50*: 184-200.